Masters Theses | Student Theses and Dissertations

Spring 2019

High-speed PCB trace design using a behavioral surface roughness model and high-speed test coupon design with non-functional pads

Han Gao

Follow this and additional works at: https://scholarsmine.mst.edu/masters_theses

Part of the Electrical and Computer Engineering Commons

Department:

Recommended Citation

Gao, Han, "High-speed PCB trace design using a behavioral surface roughness model and high-speed test coupon design with non-functional pads" (2019). *Masters Theses*. 7884.
https://scholarsmine.mst.edu/masters_theses/7884

HIGH-SPEED PCB TRACE DESIGN USING A BEHAVIORAL SURFACE

ROUGHNESS MODEL AND HIGH-SPEED TEST COUPON DESIGN WITH NON-

FUNCTIONAL PADS

by

HAN GAO

A THESIS

Presented to the Faculty of the Graduate School of the

MISSOURI UNIVERSITY OF SCIENCE AND TECHNOLOGY

In Partial Fulfillment of the Requirements for the Degree

MASTER OF SCIENCE IN ELECTRICAL ENGINEERING

2019

Approved by:

Dr. James L. Drewniak, Advisor
Dr. Victor Khilkevich, Co-Advisor
Dr. Jun Fan

ABSTRACT

In high-speed digital systems as data rates increase to tens of gigabits per second, the loss from the conductor surface roughness cannot be ignored. Djordjeic and Huray roughness model is widely used to count for the conductor roughness loss. However the practical application of the existed models are not straight forward since the frequency-dependent dielectric loss is usually unknown, leading to high discrepancies at high frequencies (above 10 GHz). To solve this problem, a behavioral model was developed by adding a dispersive term to the dielectric. The dispersive term in the model captures dispersion behavior observed in the measurement accurately. The proposed model is validated by measurement on both single-ended and differential transmission lines. Based on behavioral model, another physic dielectric model with dispersive term added to bulk dielectric used together with the Huray surface roughness model to represent the loss due to roughness on traces.

Based on the theory proposed above, a new method to extract Dielectric constant (Dk) and dissipation factor (Df) is developed. According this new method sensitivity study, when transmission lines are tighter coupled, the more accurate of the extracted results. However, most of the industries test coupon are built with loss coupling. Therefore, a strong coupling test coupon with working frequency up to 50GHz need to build to verify this new extraction method. During optimization of footprint, non-functional pads are applied to reduce high impedance caused by current loops, especially for the last several bottom layers.

ACKNOWLEDGMENTS

I would like to sincerely express my gratitude to Dr. James Drewniak, my adviser, for teaching me to be rigorous and responsible, for and teaching me great skills in doing research. I am thankful for his warm encouragement when I was facing difficulties in projects and life. He provided great support to my study during the master's degree and enlightened my way to the future.

I would like to thank Dr. Victor Khilkevich, my co-adviser, for his patient, kind instructions and directions for this thesis, especially for walking me through the beginning.

I would like to thank Dr. Jun Fan for his teaching in my courses, helpful suggestions on my studies, and providing great inspiration to my academic and career path. He gave me a lot of support during my study.

I would like to express my thanks to all other faculty members and students in the EMC lab for their help. It has been a great pleasure to be a member of the lab.

TABLE OF CONTENTS

LIST OF ILLUSTRATIONS

LIST OF TABLES

1. INTRODUCTION

Nowadays, several models are proposed to model dielectric in PCB boards. The most popular one is Djordjevic model[4], which is a causal model because it meets K-K relationship. However, a majority issue of this model is it can't model insertion loss at both low frequency and high frequency accurately, as shown in Figure 1.1. This discrepancy might not too much when look at frequency domain. However, when look at time domain, this discrepancy may cause issues in time domain: jitter, which could kill systems by SI issues. A behavior model[5] is proposed recently to model insertion loss accurately in both frequency domain and time domain. However, the main limitation of this method is it can only apply to low loss material. Once dissipation factor is greater than 0.09, insertion loss will be overestimated. Inaccurate material property modeling could introduce SI PI modeling issues, inaccurate de-embedding results [21]-[32].
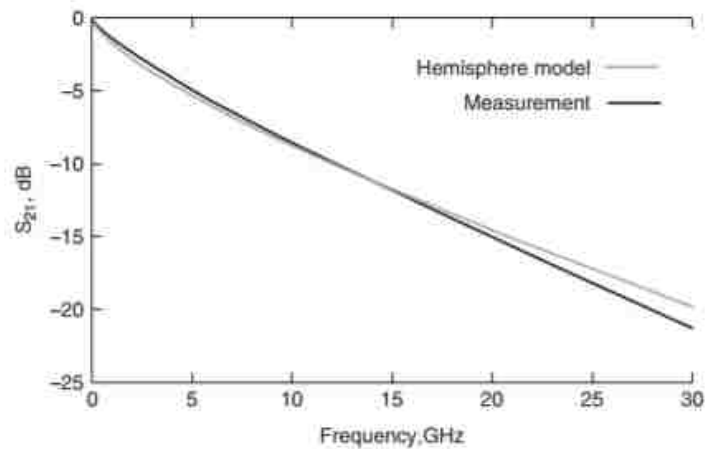
Figure 1.1. Comparison between Measurement |S_{21}| and Hemisphere model |S_{21}| in dB.

In addition, multiple models are proposed to model surface roughness on copper: hammerstad model, hemispherical model and huray model. The correction factors from three models are comparing in Figure 1.2. The major issue for hammerstad model is once surface roughness in rms value is greater than 2um, roughness factor will be saturated which will lead loss underestimated. Based on hammerstad model, hemispherical model is proposed. Hemispherical correction factor is calculated by the ratio of then power absorbed with and without a good conducting [6]. Another popular model, huray model, is used in industry. Based on [6], hemisphere model overestimates roughness at low frequency and underestimates at high frequency. Only huray factor provides an accurate estimation. Therefore, huray model will be used to model surface roughness in this paper.
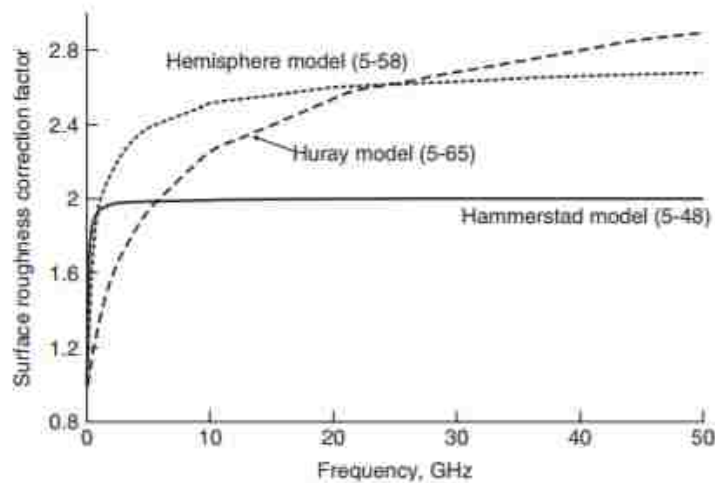
Figure 1.2. Surface roughness correction factor comparison among Hammerstad model, Hemisphere model and Huray model.

In Section 2, a high-speed PCB board with strong coupling traces are designed. During via-transition optimization, a high impedance caused by current loops between

signal via and GND vias cannot be removed following regular optimization flow. Therefore, a new technique: non-functional pads are added to top layers to help reduce this high impedance.

2. BACKGROUD STUDY

2.1. POSSIBLE PHYSICS OF ANOMALOUS OF |S21| BEHAVIORAL

According to Hemispherical model of roughness, as shown in Figure 2.1, power scatted and absorbed by a sphere divided by incident flux is known as total radar cross-section, as shown in Equation (1). The total radar cross-section of sphere is summation over a spherical harmonics.
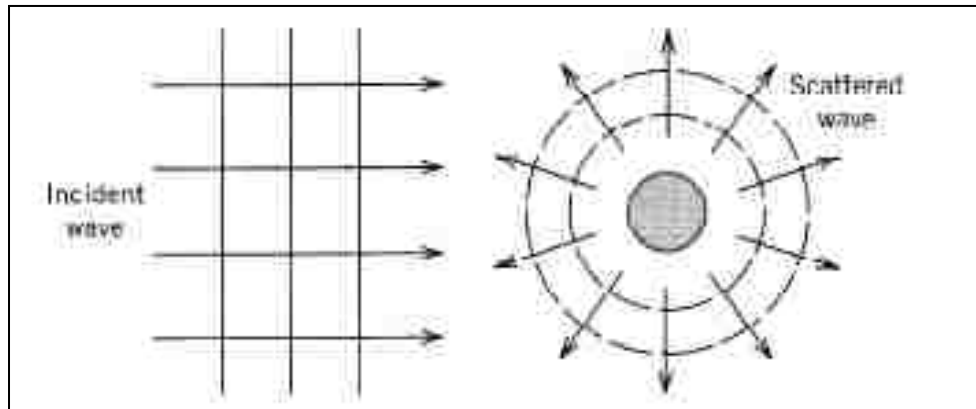
Figure 2.1. Incident wave and scattered wave on a sphere.

$$\sigma_t = -\frac{\pi}{k^2}\sum_l(2l+1)Re[\alpha(l)+\beta(l)] \tag{1}$$

where k=2π/λ, $\lambda = \frac{c}{f\sqrt{\varepsilon'}}$, c is the speed of light. The scattering coefficients are approximated assuming that kr << 1, where r is the sphere radius and are given by[2]. Therefore, based on the equation above, total radius power against with frequency can plot as in Figure 2.2.
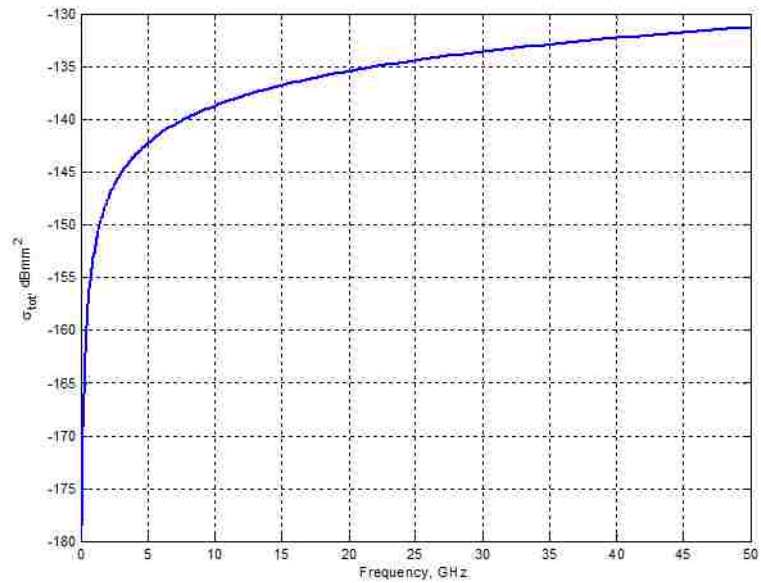
a
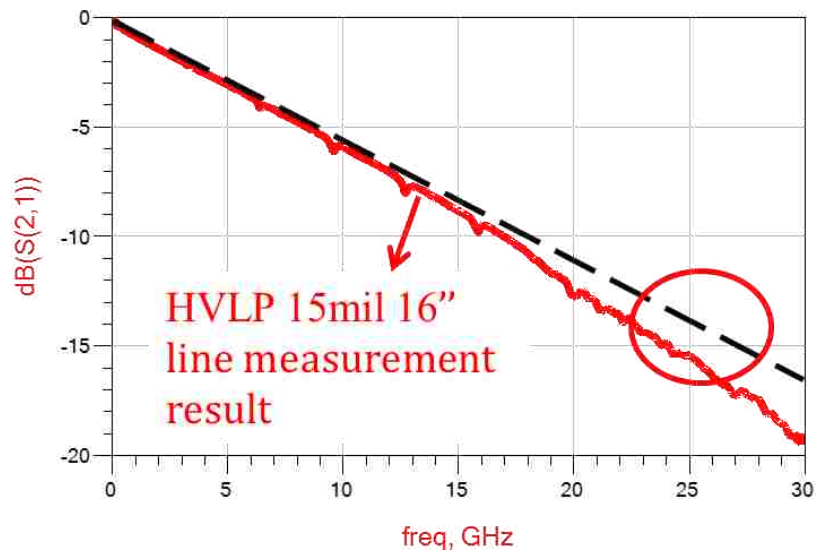
b

Figure 2.2. Total radiation power and measured insertion loss. a) Total radiation power with 5µm sphere. b) Measured S-parameter with a 16in transmission line.

As shown in Figure 2.2, when frequency goes up above 10GHz, total radar cross-section is behaved quasi-linear. Therefore, roughness couldn't explain why we have discrepancy between measurement and expectation (at high frequency, measured S-parameters has frequency-depended behavior).

"Over the last decade or so there has been a continuous shift away from the traditional oxides and reduced oxides to what is generally referred to as oxide alternatives or OAs. OAs are essentially highly modified etchants that impart a rough surface to the copper via a complex set of chemical reactions and results in a uniform, thin micro-roughened, organo-metallic surface"[3]. From this paragraph, another assumption can be made that the frequency-depended behavior in S-parameter may come from the coating on the surface. To verify this assumption, a simulation is CST is done.
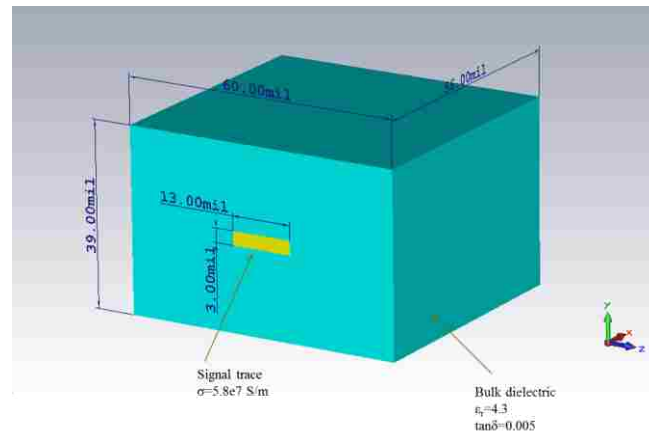
a

Figure 2.3. Geometries and port setting in CST simulation. a) Transmission line geometries. b) Ports and boundary settings. c) Trace geometries. d) Periodic rectangular shape and additional thin dielectric.
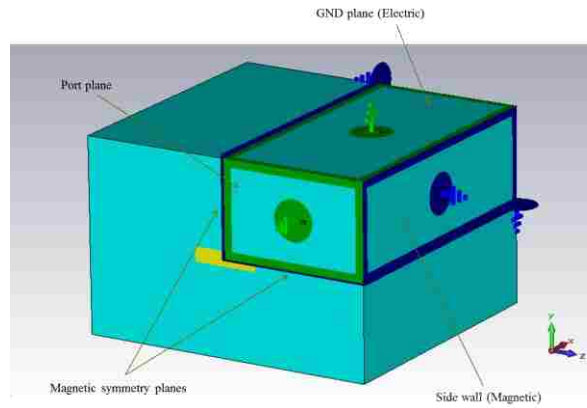
b
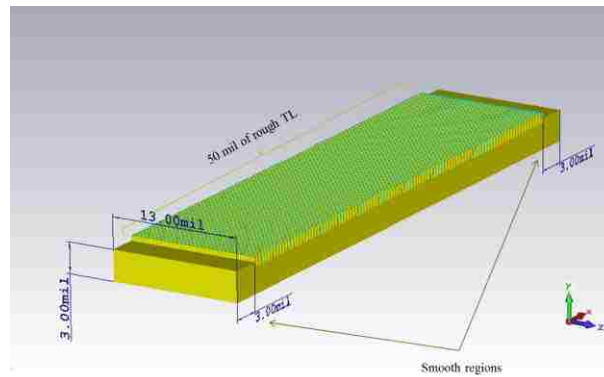
c
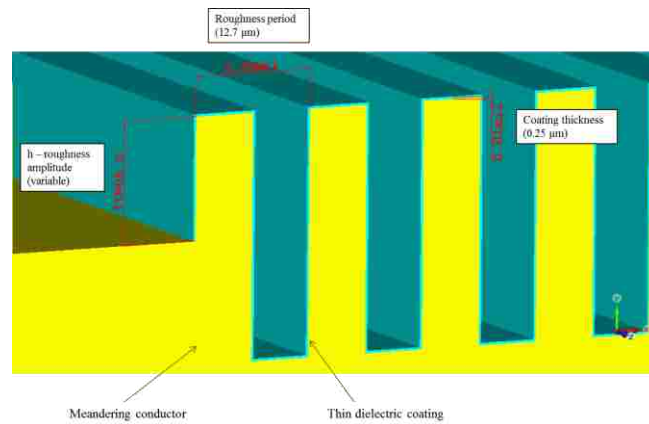
d

Figure 2.3. Geometries and port setting in CST simulation. a) Transmission line geometries. b) Ports and boundary settings. c) Trace geometries. d) Periodic rectangular shape and additional thin dielectric. (Cont.)

As shown in Figure 2.3, a 56mil transmission line is built in CST. Trace width is 13mil and trace thickness is 3mil. Dielectric has total thickness 39mil and filed with material Dk=4.3 and Df=0.005. All those geometries make sure the transmission line is 50Ohm. Two PEC boundaries are assigned to top and bottom side as the ground layers in transmission line. Magnetic symmetric walls are assigned to the inner side walls. This setting will highly save simulation running time. Ports are set at front and back faces.

To simulate roughness on the trace, periodic rectangular shapes with 0.5mil height along trace surface are created. In addition, another 0.01mil coating is added on the surface. By using Debye first order model to dielectric coating, ε_{dc} is assigned to be 20 and ε_{inf} is assigned to be 3. This relatively high permittivity and loss behaviors are shown in Figure 2.4.

a   b
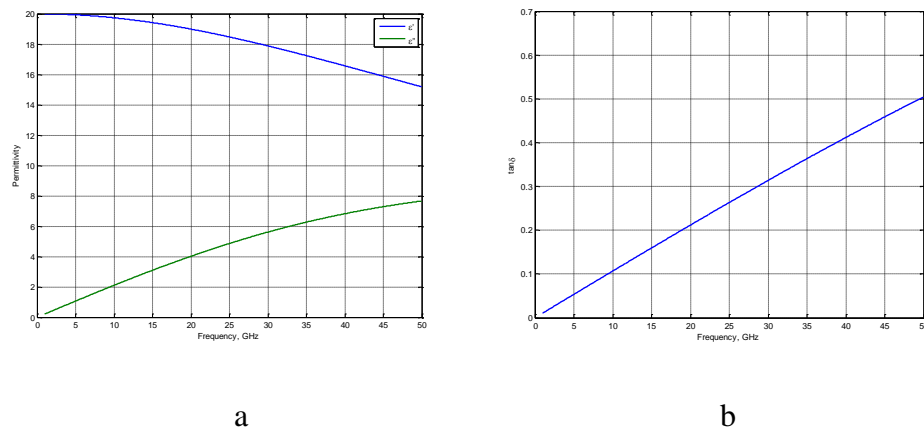
Figure 2.4. Properties of the additional dielectric layer. a) Real and imagine part of the addition dielectric layer. b) tanδ for the addition dielectric layer increasing with frequency.

From Figure 2.4, Df is increasing linearly with frequency. Therefore, what we observed in Figure 2.2 can't explain the loss frequency-depended behavior in S-parameters. Thus, ω^2 term should be expected in $|S_{21}|$ curves.

As Figure 2.5 show, loss at 50GHz is still less than -0.12dB due to extremely short transmission line. This will lead to the return loss is comparable to the loss in the transmission line. Therefore, accepted loss is used instead of S_{21}.the accepted loss equation is shown in Equation (2).
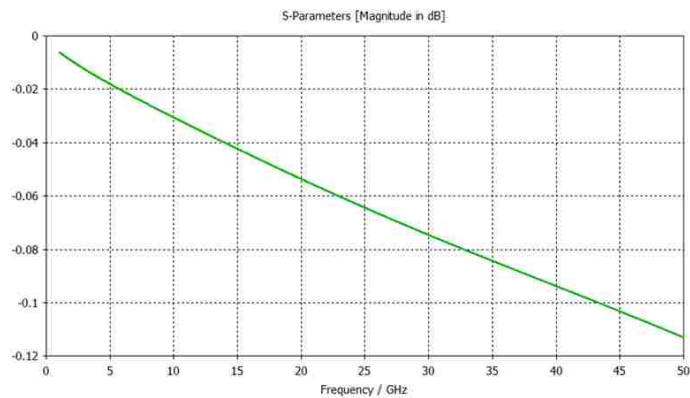
a
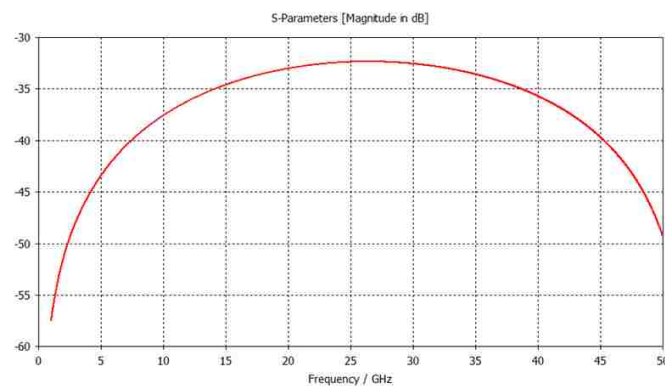
b

Figure 2.5. Simulated S-parameters. a) Simulated insertion loss ($|S_{21}|$). b) Simulated return loss ($|S_{11}|$).

$$P_{acc} = |S_{11}|^2 + |S_{21}|^2 \tag{2}$$

Simulations are done from total smooth case to very roughness cases. H_{rms} values

are used to present roughness level, which is defined as rms value of roughness peaks.

$$h_{rms} = \sqrt{\frac{1}{n}\Sigma_1^n x_i^2} \tag{3}$$

where n is the number of peaks and x_i is value of the ith peak. All accpeted loss are

shown in Figure 2.6. Peak values and rms values for differential foil types are list in

Table 2.1.
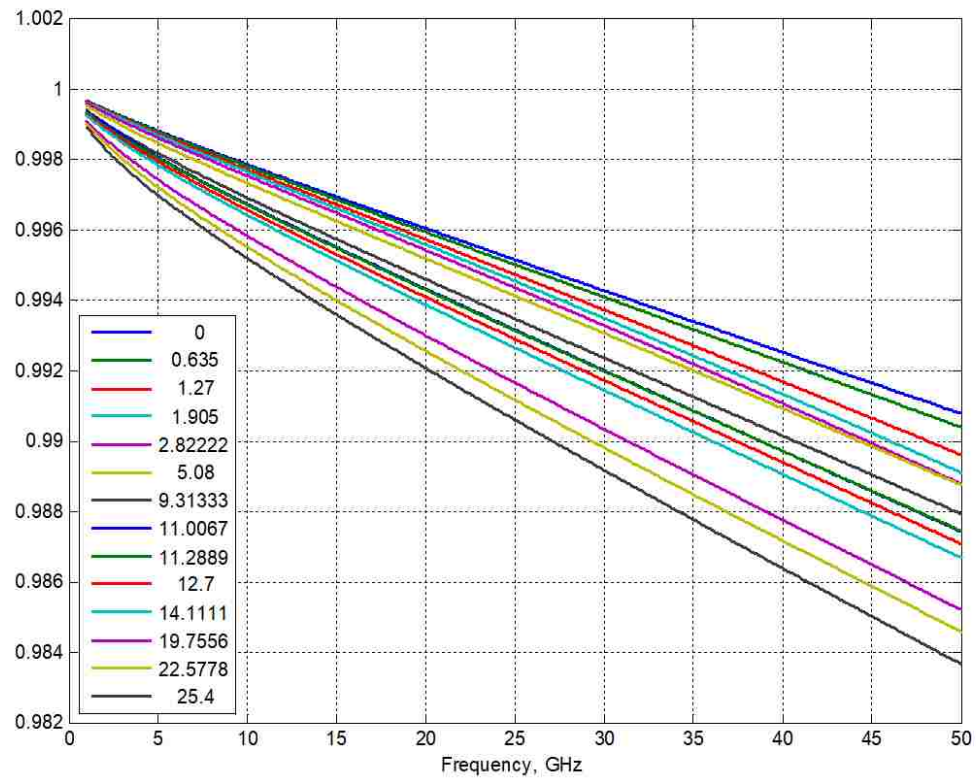
Figure 2.6. Accepted loss with surface roughness sweeping from 0 to 25.4µm.

Table 2.1. Surface roughness range for different foil types.

Resist Side	h_{rms}, µm	Peak to Peak, µm
STD	1.0-2.0	7.0-12.0
VLP	0.3-0.4	3.0-4.0
HVLP	0.25-0.35	2.0-3.0
After alt. Oxide	h_{rms}, µm	Peak to Peak, µm
STD	1.0-2.0	7.0-12.0
VLP	0.6-1.0	6.0-8.0
HVLP	0.5-0.7	4.0-6.0

a   b
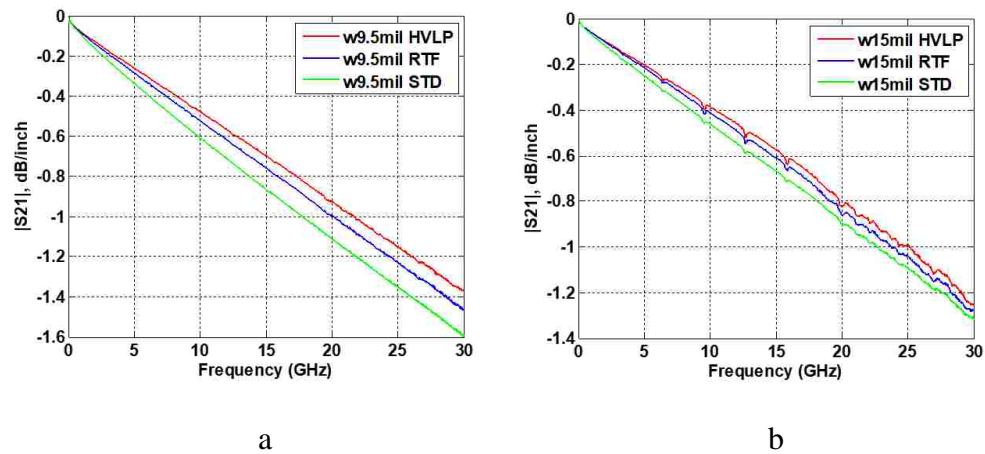
Figure 2.7. Measured insertion loss with trace width 9.5mil and 15mil with HVLP, RTF and STD foil type. a) 9.5mil trace width with different foil type. b) 15mil trace width measurements with different foil types.

From Figure 2.6, when surface roughness is moderate, the frequency depended behavior is obviously. ω^2 term increases with roughness. In addition, contribution of the ω^2 term decrease and eventually the linear term dominates. Finally, when roughness

effect is pretty strong, there is no ω^2 behavior can be observed. By comparing with

measured S-parameters on Megtron6 with trace width 9.5mil and 15mil, which are shown

in Figure 2.7, when foil type is HVLP, the frequency-depended behavior is significantly

observed and when foil type change to STD, such behavior is vanished. Therefore, we

can make the conclusion that this additional dispersive lossy layer could be a reason for

the anomalous behavior of $|S_{21}|$.

2.2. ROUGHNESS CALCULATION BASED ON CROSS-SECTION

A simulation is done to investigate how does surface roughness impact insertion

loss, especially when foil side and oxide side have different surface roughness value.
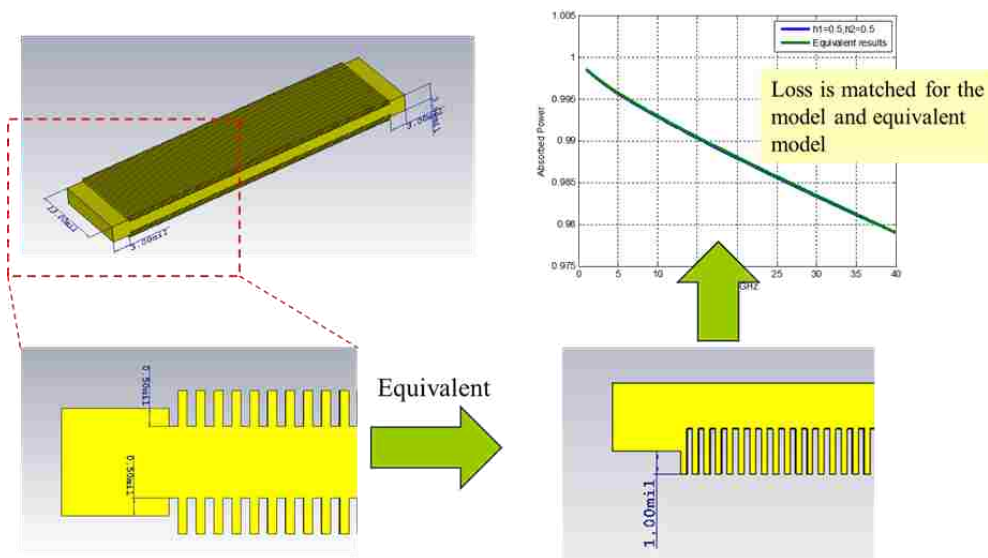
Figure 2.8. Equivalent roughness calculation on foil side and oxide side.

A several group of simulation are down and the results show that the height of surface roughness has linear relationship because accepted power (insertion loss) is exactly same with two cases, as shown in Figure 2.8 and Figure 2.9. Therefore, to model surface roughness in real cases, both foil side and oxide side surface roughness should be considered, and the simplest way to do it is take average of both side.
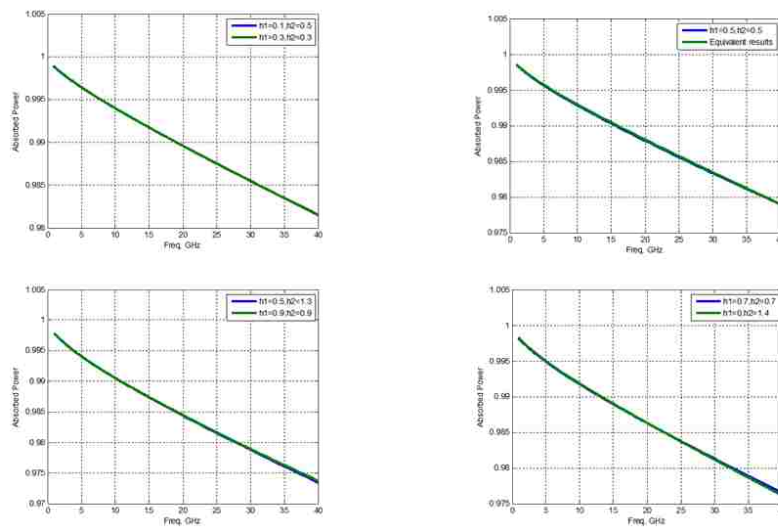
Figure 2.9. Comparison equivalent roughness calculation among four different surface roughness.

2.3. DISPERSIVE BEHAVIOR IN REAL MATERIALS

Not only the coating on surfac of trace has dispersive behavior, dielectric can also observed dispersive behavior.A measurement was done with dieletric materal DS7409D(VN) with splite post dielectric resonators (SPDR). Measuements are done under 10GHz, 15GHz and 21.5GHz. Dk and Df measured results are shown in Table 2.2.

By doing curve fitting over frquency range 0Hz to 50GHz, obvious dispersion is observed in Df against frequency, as shown in Figure 2.10.

Table 2.2. Measured Dk and Df from SPDR method.

Resonance Freq	10GHz	15GHz	21.5GHz
Dk	3.34	3.34	3.35
Df	0.0019	0.0023	0.0027
Dielectric Loss [dB/in]	0.16	0.29	0.49
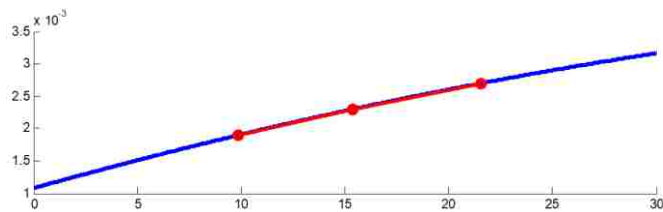
Figure 2.10. Measured Df on 10GHz, 15GHz and 21GHz and curve fitting along frequency from 0Hz to 50GHz.

Based on the background studies, the can make conclusions that material that build PCB boards have obvious dispersions. In addition, not only materials, the treatment on oxide of traces, which will lead to an addition lossy dielectric layer will also cause dispersions.

3. BEHAVIORAL MODEL

3.1. MODEL DESCRIPTION

In an earlier study [4], a practical causal approximation for low-dispersive

dielectrics often used in the PCBs (Djordjevic model [5]) is presented. The dielectric

constant was calculated as Equation (4) and (5).

$$\text{Re}\{\varepsilon_r(\omega)\} = \varepsilon' \approx \varepsilon'_\infty + \frac{\Delta\varepsilon\prime}{m_2 - m_1} \frac{ln\left(\frac{\omega_2}{\omega}\right)}{\ln(10)} \tag{4}$$

$$\text{Im}\{\varepsilon_r(\omega)\} = \varepsilon'' \approx \frac{\Delta\varepsilon\prime}{m_2 - m_1} \frac{-\frac{\pi}{2}}{\ln(10)} \tag{5}$$

Besides the dielectric parameters ε'_∞ and $\Delta\varepsilon'$, the model is characterized by two

frequency limits $\omega_1 = 10^{\omega_1}$ and $\omega_2 = 10^{\omega_2}$. Usually the lower frequency limit is set to a

kHz value and the upper one is set to a THz value. This allows generating the causal

dielectric constant function that is practically constant in the frequency range of interest

of typical signal integrity simulations (MHz – tens of GHz). Most of the dielectrics used

for PCB manufacturing are indeed very low-dispersive (at least starting from 5-10 GHz)

[6 - 12]. However as was indicated above, the low-loss transmission lines, often exhibit

an increase in the slope of the insertion loss (S$_{21}$) curve with frequency, which cannot be

accounted by the existing models.

Although typical PCB dielectrics have low dispersion, it is possible to model the

frequency-dependent slope of S$_{21}$ by adding an effective dispersive dielectric term to the

bulk dielectric, accounting for the roughness effect in this manner.

In the proposed model, the bulk dielectric of the transmission line is calculated as

$\varepsilon_{tot} = \varepsilon_1 + \varepsilon_2$, as shown in Figure 3.1, where both terms ε_1 and ε_2 are calculated

according to Djordjevic (as shown in Equations 1 and 2). The first term is non-dispersive and describes the 'nominal' behavior of the dielectric and the second term is dispersive and accounts for the roughness effect, as shown in Figure 3.1.
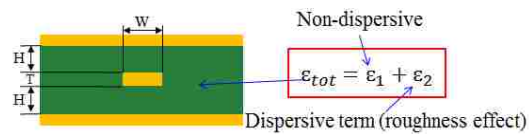
Figure 3.1. Total dielectric constant is contributed by non-dispersive term and dispersive term.

The parameters of the non-dispersive term ε_1 are calculated by specifying the desired values of ε' and tanδ at a certain frequency, and using the frequency limits ω_1 and ω_2 in the kHz and THz frequency range correspondingly.
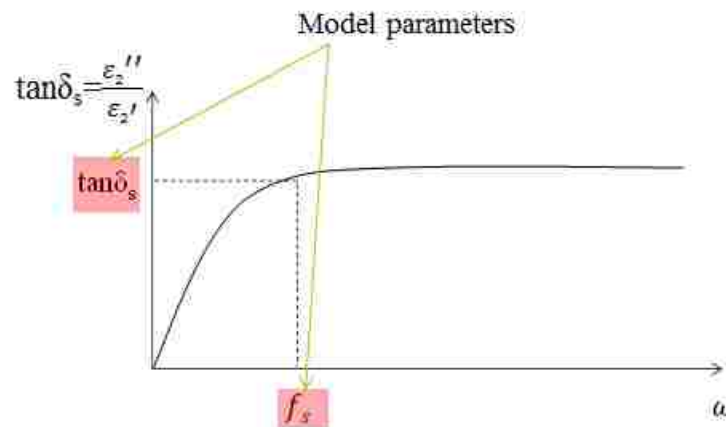
Figure 3.2. Model parameters for behavioral model.

Similar procedure is applied to calculate the dispersive part ε_2 with the following exceptions: the ε_2' is set such that $\varepsilon_2' \ll \varepsilon_1'$ (in the examples below, ε_2' is set to 0.1 for ε_1' $\approx$4); the lower frequency limit $\omega_1 = 2\pi f_s$ is set in the GHz frequency range; and tanδs is specified at the lower frequency limit. The two parameters of the dispersive term (tanδs and f_s) are illustrated in Figure 3.2.

In summary, the procedure to calculate bulk dielectric term and dispersive term are illustrated in Figure 3.3.
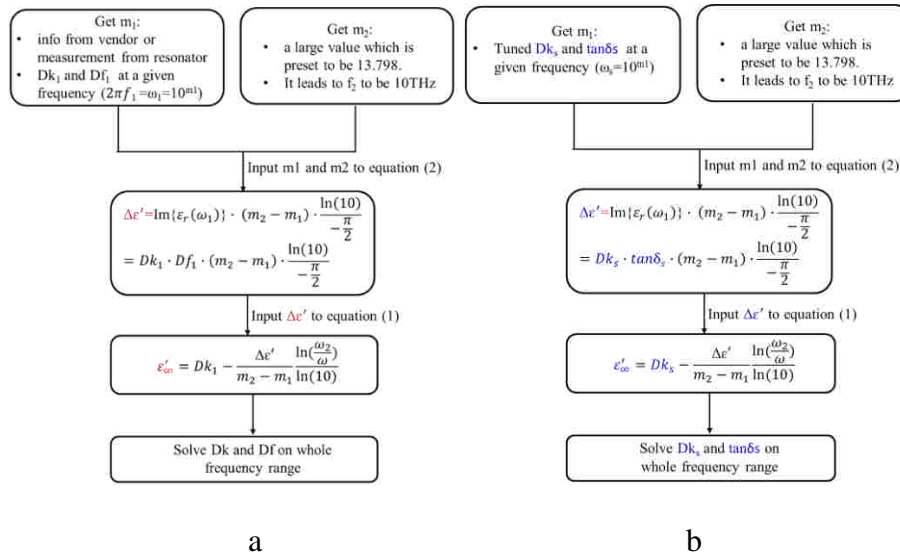
Figure 3.3. Flow chart to calculate non-dispersive term and dispersive term.

Figure 3.4 shows an example for bulk dielectric ε_{tot} plot that was calculated using this method. The non-dispersive term had nominal values of DK and DF of 3.8 and 0.006 respectively. The lower frequency limit for the non-dispersive term is 10 kHz and the

upper one is 1 THz. For the dispersive term tanδs =0.12 and fs=9 GHz. As shown in

Figure 3.5, the proposed method allows generating the causal permittivity function that

has almost frequency independent real part (Dk) and at the same time frequency

dependent loss tangent (tanδ), the parameters of which can be set independently of Dk.
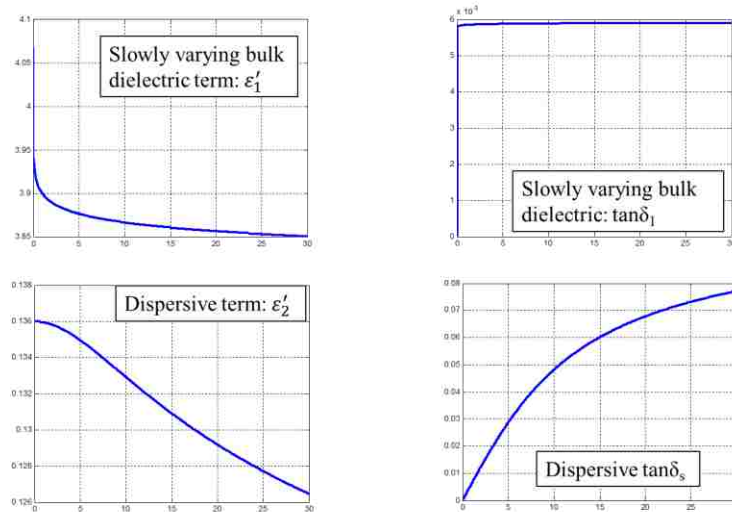
Figure 3.4. Modeled non-dispersive term and dispersive term against frequency.
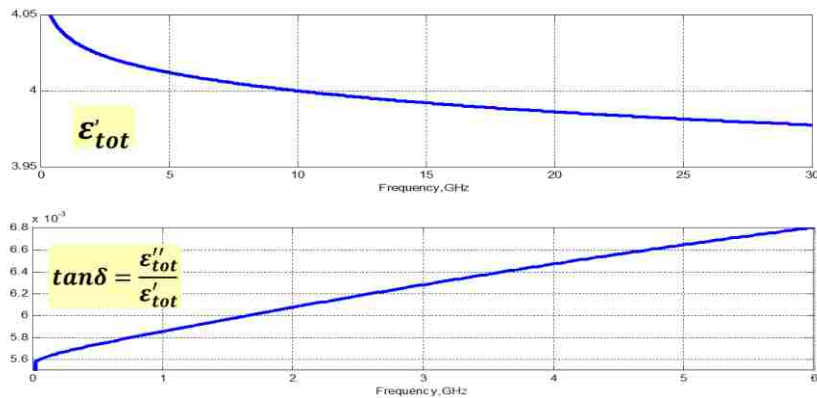
Figure 3.5. Modeled total dielectric constant and dissipation factor.

After the permittivity function is generated, the transmission coefficient of the stripline is calculated analytically based on an earlier study [13 - 14].

3.2. MODEL PARAMETERS EXTRACTION

The proposed model requires two parameters: f_s and $\tan\delta s$, both of which depend on the roughness and the geometry of the stripline. These parameters are determined empirically. For this study, a set of test vehicles (TV) were created, an example is shown in Figure 3.6. The set consisted of twelve boards, each having 50 ohm single-ended 16 inch striplines of three different roughness grades (STD, RTF/VLP, and HVLP) and four different widths (3.5, 9.5, 13 and 15 mils). All the boards contained a TRL pattern for de-embedding purposes and were manufactured using the same dielectric material (Megtron 6). An example of the test vehicle is demonstrated in Figure 3.6. For each TV, a model was built as described above, using known values for the bulk dielectric permittivity (ε_1'=3.8) and loss tangent ($\tan\delta s$ =0.006).

The parameters of the dispersive layer fs and $\tan\delta s$ were tuned for each case to ensure the best match between the measured and calculated transmission coefficients. The transmission coefficient curves along with the tuned parameters are shown in Figure 3.7.
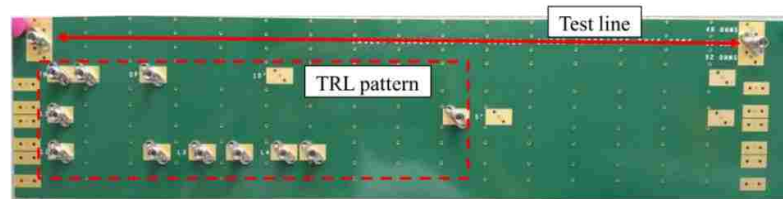
Figure 3.6. Test vehicle to do parameter extraction.
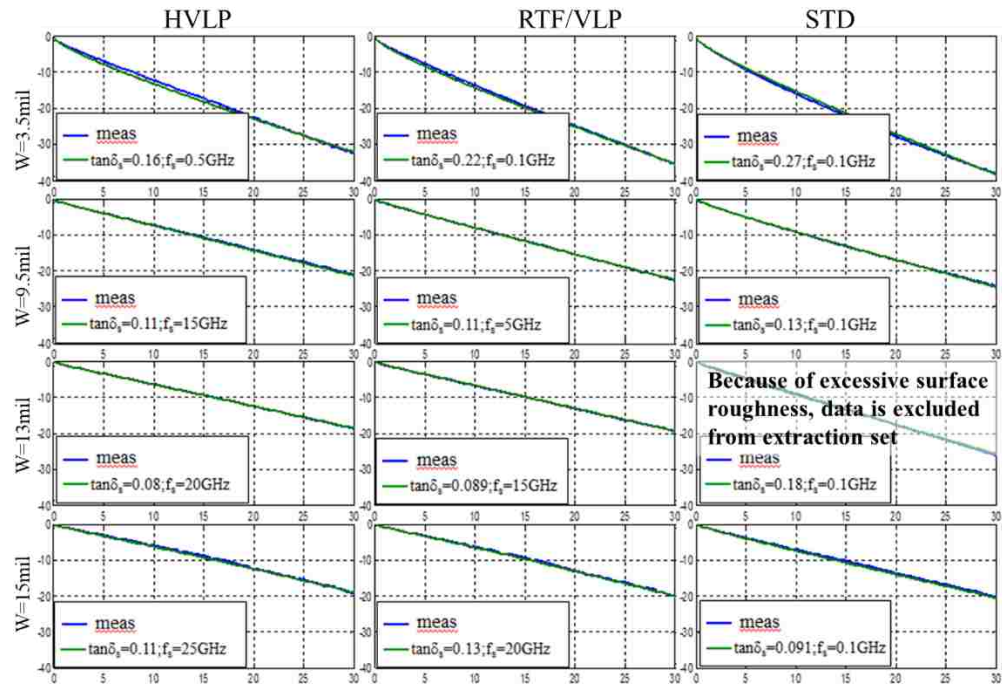
Figure 3.7. Parameters extraction with different foil type and different trace width on Megtron6 test vehicles.

The extracted parameters of the dispersive term are shown in Figure 3.7, along with the polynomial fitted approximation (design curves), which are illustrated in Figure 3.8, Figure 3.9 and Figure 3.10. The obtained design curves allow determining the dispersive term parameters for arbitrary line width, provided that the roughness of the modelled transmission-line resembles one of the roughness grades (STD, RTF/VLP, HVLP) used for the parameter extraction.

The design curves were extracted for the Megtron6 dielectric material. However these can be extended to be used for other low-loss materials, using the normalization schematic as shown in Equation (6).

$$\tan\delta_{s\_other} = \frac{\tan\delta_{0\_other}}{\tan\delta_{0\_meg6}} \tan\delta_{s\_meg6} \tag{6}$$

where $tand_{0\_meg6}$ is the value from design curve for Megtron6 board, $tand_{0\_other}$ is the

other material dispersive term dielectric loss, $tand_{0\_meg6}$ is the loss tangent for the

Megtron6 and $tand_{0\_other}$ is the loss tangent for the other material.
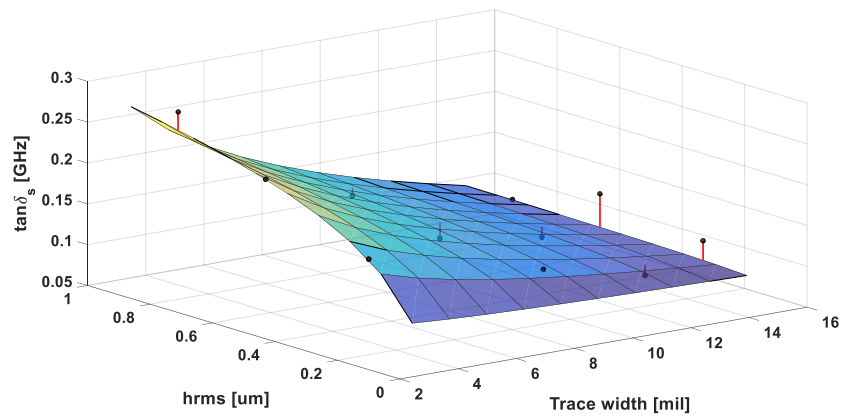
a
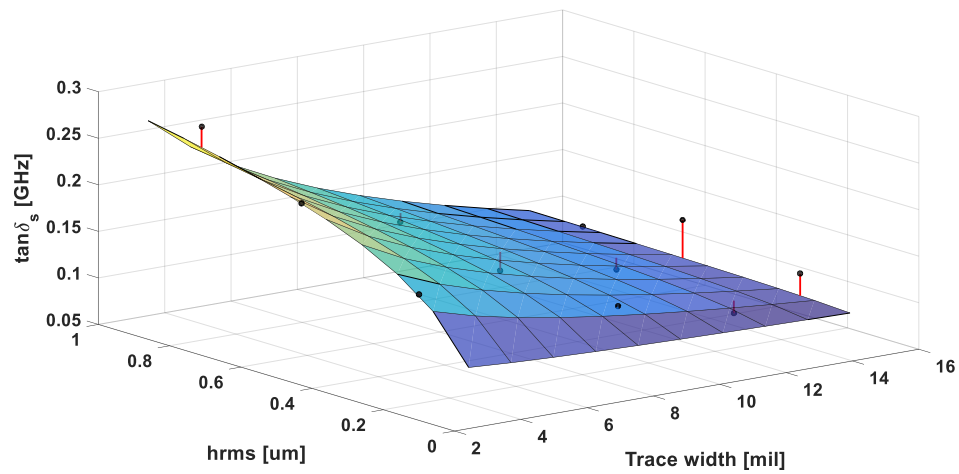
b

Figure 3.8. Surface fitting for model parameters. a) Surface fitting for tanδs. b) Surface
fitting for fs.

$$tan\delta_s = 0.4047 - 0.267log_{10}(Width) + 0.08898log_2(h_{rms}) - 0.07389(log_{10}(Width)\ log_2(h_{rms}))$$
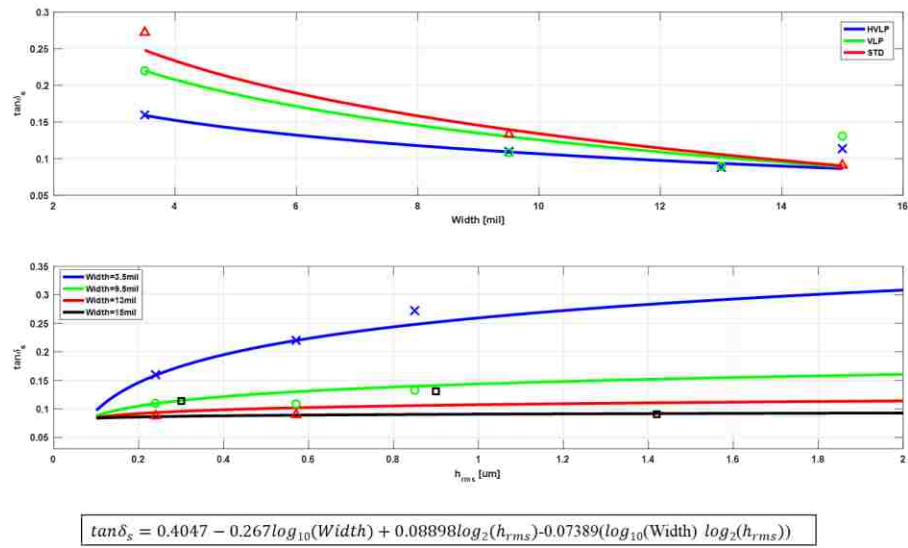
Figure 3.9. Cross-section view for tanδs and fitting equation. a) tanδs against trace width.
b) tanδs against surface roughness.

$$f_s = -0.7779 + 1.518log_{10}(Width) + 42log_{10}(h_{rms}) - 74.31(log_{10}(Width)log_{10}(h_{rms}))$$
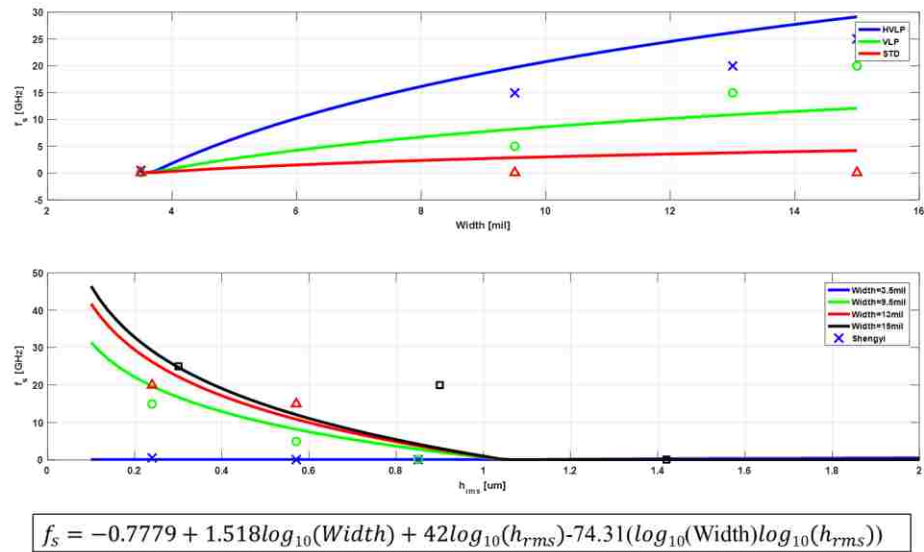
Figure 3.10. Cross-section view for fs and fitting equation. a) fs against trace width. b) fs against surface roughness.

3.3. DIFFERENTIAL TRANSMISSION LINE PARAMETERS CALCULATION

To calculate S-parameters, a general way to do is calculating p.u.l RLGC term

then propagation constant can be obtained.

3.3.1. Even And Odd Mode P.U.L RLGC Calculation. According to Equation

(7) and (8) [15], even mode and odd mode impedance can be calculated separately.

$$Even\ mode: Z_{0e}(\frac{w}{b},\frac{t}{b},\frac{s}{b}) = \{\frac{1}{Z_0\left(\frac{w}{b},\frac{t}{b}\right)} - \frac{C_f{'}\left(\frac{t}{b}\right)}{C_f{'}(0)}[Z_0\left(\frac{w}{b},0\right) - \frac{1}{Z_{0e}\left(\frac{w}{b},0,\frac{t}{b}\right)}]\}^{-1} \qquad (7)$$

$$Odd\ mode: Z_{0o}(\frac{w}{b},\frac{t}{b},\frac{s}{b}) = \{\frac{1}{Z_0\left(\frac{w}{b},0,\frac{t}{b}\right)} + \left[\frac{1}{Z_0\left(\frac{w}{b},\frac{t}{b}\right)} - \frac{1}{Z_0\left(\frac{w}{b},0\right)}\right] - \frac{2}{377}\left[\frac{C_f{'}\left(\frac{t}{b}\right)}{\varepsilon} - \frac{C_f{'}(0)}{\varepsilon}\right] + \frac{2t}{377s}\}^{-1}$$

$$(8)$$

Considering about fringing field, p.u.l capacitance for even mode and odd mode

can be calculated as [15].

$$Even\ mode: C_f{'}\left(\frac{t}{b}\right) = \frac{\varepsilon}{\pi}[\frac{2}{1-\frac{t}{b}}ln\left(\frac{1}{1-\frac{t}{b}}+1\right) - \left(\frac{1}{1-\frac{t}{b}}-1\right)ln(\frac{1}{\left(1-\frac{t}{b}\right)^2}-1)] \qquad (9)$$

$$Odd\ mode: C_f{'}\left(\frac{t}{b}\right) = \frac{\varepsilon}{\pi}[\frac{2}{1-\frac{t}{b}}ln\left(\frac{1}{1-\frac{t}{b}}+1\right) - \left(\frac{1}{1-\frac{t}{b}}-1\right)ln(\frac{1}{\left(1-\frac{t}{b}\right)^2}-1)] \qquad (10)$$

Therefore, based on impedance calculated related to geometries with fringing

field considered, we can calculate p.u.l inductance (L), capacitance (C) and conductance

(G) by [1].

$$C = \frac{1}{vZ_0} \qquad (11)$$

$$L = CZ_0^2 \qquad (12)$$

$$G = C\omega \tan\delta \qquad (13)$$

The last transmission line parameter left is per unit length resistance (p.u.l R). According to single-ended model parameter calculation, we can calculate resistance on trance and ground separately by [1]:

$$R_{trace} = \frac{1}{2w}\sqrt{\frac{\pi\mu f}{\sigma}} \tag{14}$$

$$R_{ground} = \frac{1}{6h}\sqrt{\frac{\pi\mu f}{\sigma}} \tag{15}$$

For differential transmission line, we also need to consider proximity effect. According to Equation (15), proximity effect correction factor for odd mode can be calculated as [16]:

$$proximity\ correction\ factor = \frac{1}{\sqrt{1-(\frac{w}{s+w})^2}} \tag{16}$$

Therefore, to calculate p.u.l resistance, we can follow Equation (17) and (18).

$$Even\ mode:\ R_{even} = \frac{1}{6}\sqrt{\frac{\pi\mu f}{\sigma}}\left(\frac{3}{w}+\frac{1}{h}\right) \tag{17}$$

$$Odd\ mode:\ R_{odd} = \frac{1}{6}\sqrt{\frac{\pi\mu f}{\sigma}}\left(\frac{3}{w}+\frac{1}{h}\right)\times proximity\ effect\ correction\ factor$$

$$\tag{18}$$

Till now, we have already got all per unit length parameters. Therefore, we can calculate propagation constant for even mode and odd mode by Equation (19)[1].

$$\gamma = \sqrt{(R+j\omega L)(G+j\omega C)} \tag{19}$$

In addition, transmission coefficient for even and odd mode can be calculated separately as Equation (20) [1].

$$T = e^{-\gamma l} \tag{20}$$

3.3.2. Converting Even And Odd Mode Parameters To Mixed Mode. By assuming network is symmetric, as shown in Figure 3.11, we can only analyze two ports instead of four ports. The converting matrix from single-ended to mixed mode is in Equation (21) [17].
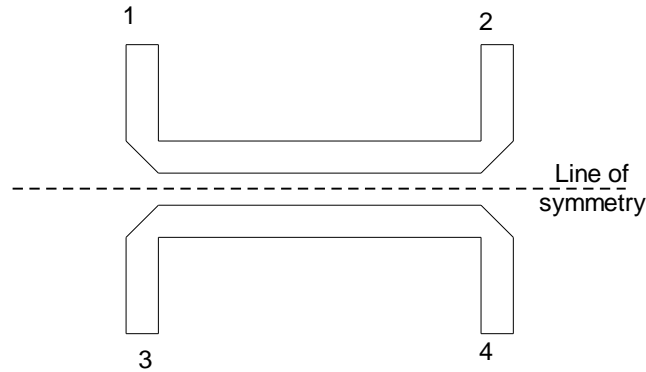
Figure 3.11. Port assignment for a symmetric transmission line model.

$$\begin{bmatrix} S_{11} & S_{12} & S_{13} & S_{14} \\ S_{21} & S_{22} & S_{23} & S_{24} \\ S_{31} & S_{32} & S_{33} & S_{34} \\ S_{41} & S_{42} & S_{43} & S_{44} \end{bmatrix} = \begin{bmatrix} S_{dd11} + S_{cc11} & S_{dd12} + S_{cc12} & -S_{dd11} + S_{cc11} & -S_{dd12} + S_{cc12} \\ S_{dd21} + S_{cc21} & S_{dd22} + S_{cc22} & -S_{dd21} + S_{cc21} & -S_{dd22} + S_{cc22} \\ -S_{dd11} + S_{cc11} & -S_{dd12} + S_{cc12} & S_{dd11} + S_{cc11} & S_{dd12} + S_{cc12} \\ -S_{dd21} + S_{cc21} & -S_{dd22} + S_{cc22} & S_{dd21} + S_{cc21} & S_{dd22} + S_{cc22} \end{bmatrix}$$

(21)

Therefore, we can get ABCD matrix by using even mode and odd mode through propagation constant by Equation (22) [17].

$$ABCD = \begin{bmatrix} \cosh(\gamma l) & Z_0 \sinh(\gamma l) \\ \dfrac{\sinh(\gamma l)}{Z_0} & \cosh(\gamma l) \end{bmatrix}$$

(22)

Using conversion with port impedance Z_0, we S-parameters is calculated from Equation (23).

$$[S] = \frac{1}{Z_0A + B + Z_0^2C + Z_0D}\begin{bmatrix} Z_0A + B - Z_0^2C - ZoddD & 2Z_0(AD - BC) \\ 2Z_0 & -Z_0A + B - Z_0^2C + Z_0D \end{bmatrix}$$

(23)

After inputting odd mode ABCD matrix in to conversion matrix, we could get

differential mode and common S-parameters as Equation (24) and Equation (25) [17].

$$\begin{bmatrix} Sdd11 & Sdd12 \\ Sdd21 & Sdd22 \end{bmatrix} =$$

$$\frac{1}{2Z0\cosh(\gamma_{odd}l) + \frac{Z_{odd}^2 + Z_0^2}{Z_{odd}}\sinh(\gamma_{odd}l)}\begin{bmatrix} \frac{Z_{odd}^2 - Z_0^2}{Zodd}\sinh(\gamma_{odd}l) & 2Z_{odd} \\ 2Z_{odd} & \frac{Z_{odd}^2 - Z_0^2}{Z_{odd}}\sinh(\gamma_{odd}l) \end{bmatrix}$$

(24)

$$\begin{bmatrix} Scc11 & Scc12 \\ Scc21 & Scc22 \end{bmatrix} =$$

$$\frac{1}{2Z0\cosh(\gamma_{even}l) + \frac{Z_{even}^2 + Z_0^2}{Z_{even}}\sinh(\gamma_{even}l)}\begin{bmatrix} \frac{Z_{even}^2 - Z_0^2}{Z_{even}}\sinh(\gamma_{even}l) & 2Z_{even} \\ 2Z_{even} & \frac{Z_{even}^2 - Z_0^2}{Z_{even}}\sinh(\gamma_{even}l) \end{bmatrix}$$

(25)

3.4. MODEL VALIDATION

For this study, twenty one cases were used to validate the behavioral model. As

shown in Figure 3.12, the validation set includes high-loss and middle-loss materials

($\tan\delta > 0.01$) as well as low-loss material ($\tan\delta \leq 0.008$), with different trace widths and

roughness. All validation set can be separated into two parts: when $\tan\delta$ is smaller than

0.009, behavioral model has better performance, which means surface roughness need to

considered when predict S_{21}; when $\tan\delta$ is greater than 0.009, behavioral model is not

needed. Otherwise, S_{21} will be overestimated when comparing with measurement results,

no matter for frequency domain or time domain.
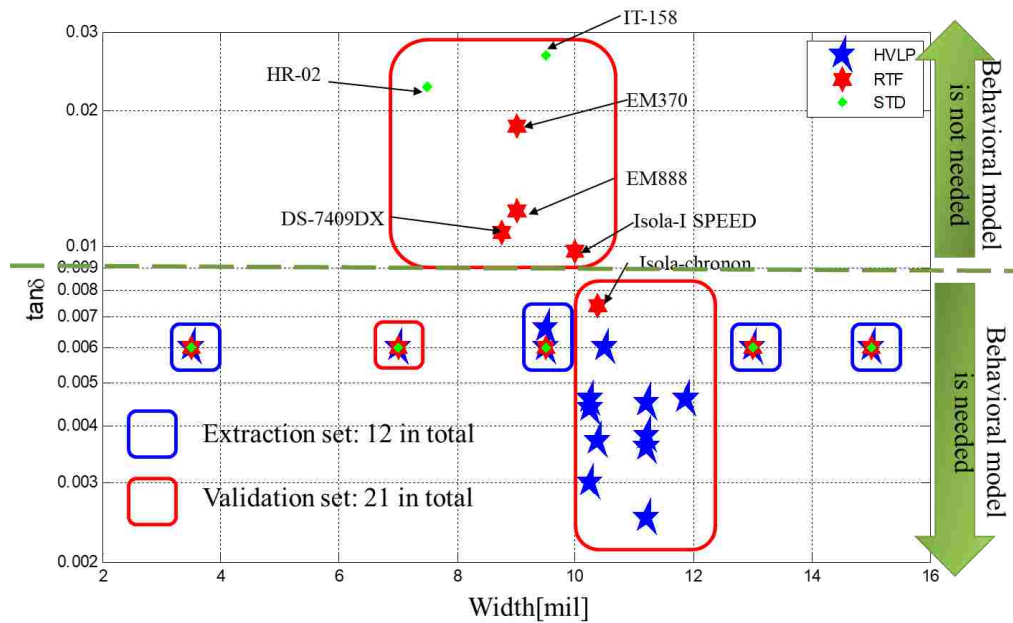
Figure 3.12. Design space for behavioral model.

3.4.1. Single-Ended Model Validation. Figure 3.13 and Figure 3.14 shows four examples of the validation of the behavioral model compared with the results obtained in ADS. Each example has different trace width, material and roughness. Peak values in millivolt from single-bit response comparing with measurements are also list in Table 3.1 and Table 3.2. Table 3.3 list all peaks values from single-bit response for validated materials and Table 3.4 compare rms error between behavioral model, ADS model and measurements. As we can see, behavioral model with surface roughness on both sides considered have better results than behavioral model with foil side surface roughness considered and ADS models. From rms error in percentage, we can see that behavioral model with average roughness has error 2.7% only when comparing with measurements.

Figure 3.13. Comparison among measurements, behavioral model and ADS model on frequency domain and time domain: Megtron7 material (single-ended).

Table 3.1. Peak value from single bit response comparison: Megtron7 (single-ended).

		Measure	BV-foil	BV-avg	ADS
Peak value (mV)	180	324.7	328.5	325.1	287.5
	181	347	363.8	361.1	318.9
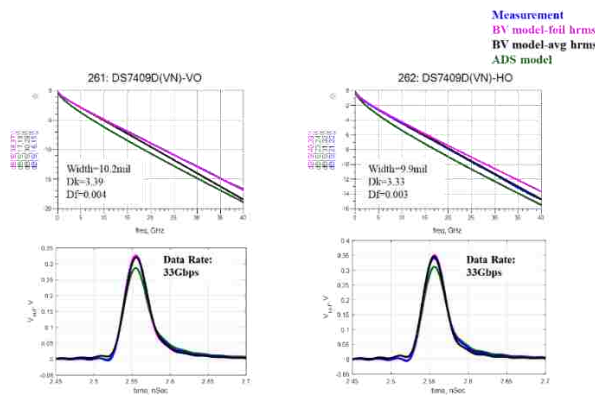
Figure 3.14. Comparison among measurements, behavioral model and ADS model on frequency domain and time domain: DVN material (single-ended).

Table 3.2. Peak value from single bit response comparison: DVN (single-ended).

		Measure	BV-before	BV-avg	ADS
Peak value (mV)	261	324.7	327	320.3	287.1
	262	340.8	350.4	345.8	311.6

Table 3.3. Peak values of single bit response comparison among validation set.

Board	Measure	BV-foil	BV-avg	ADS
MEG7E-RHV-RS	312	323	320	290
MEG7E-NHV-MF	296	302	297	270
MEG7NE-RHV-RS	324.7	328.5	325.1	287.5
MEG7NE-NHV-MF	347	363.8	361.1	318.9
DS-7409D (VN)_HVLP	302.2	317	306.3	279.7
DS-7409D(V-N)_PCF	293.3	308.5	295.1	269.5
DS-7409D(VN)_VO	324.7	327	320.3	287.1
DS-7409D(VN)_HO	340.8	350.4	345.8	311.6
TACHYON -100G VLP2	301.8	321.1	316.4	278.4
TU933	308.3	328.4	321.8	294.3

Table 3.4. Rms error based on measurement results comparison between behavioral model and ADS model.

BV-foil	BV-avg	ADS
4.23%	2.70%	8.64%

3.4.2. Differential Model Validation. Figure 3.15 and Figure 3.16 shows four examples of the validation of the behavioral model compared with the results obtained in

ADS. Each example has different trace width, material and roughness. Table 3.5 and

Table 3.6 list peak values of single-bit response for Megtron7 and DVN. Differential

mode peak values and common mode peak values are list separately. As we can see,

behavioral model with foil side and oxide surface roughness considered in model has

better results than model only have foil side roughness included only. Therefore, the

results prove again that surface roughness from both side of traces should be considered,

which is constant with the conclusion in background study.
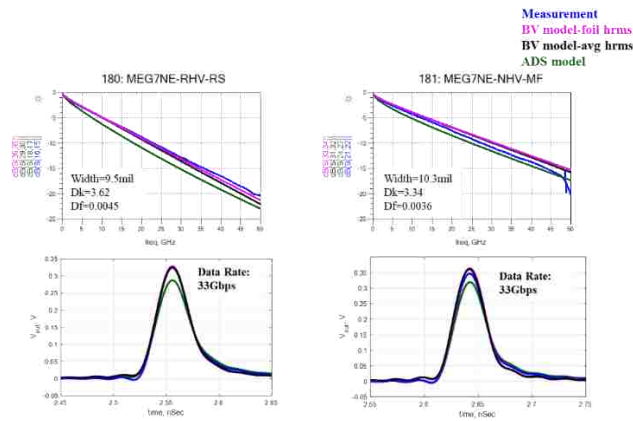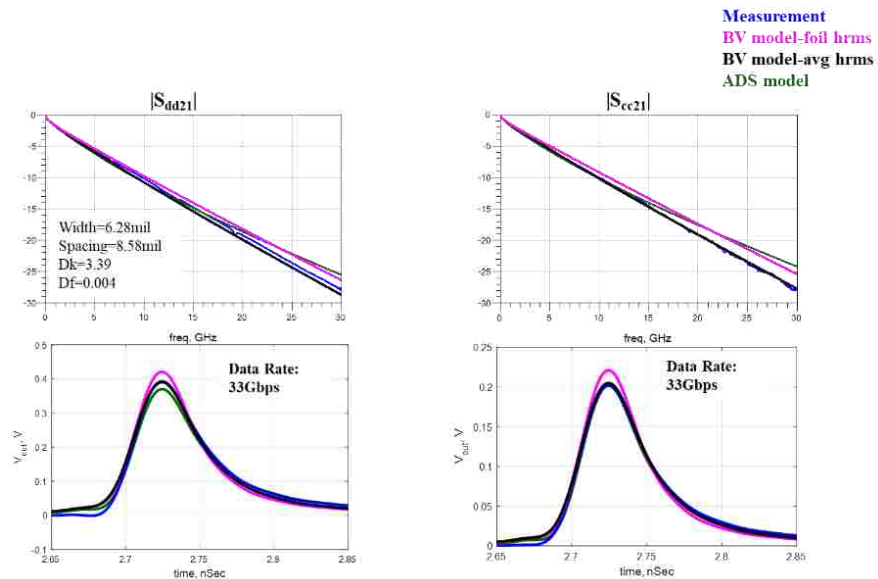

Figure 3.15. Comparison among measurements, behavioral model and ADS model on frequency domain and time domain: Megtron7 material (differential).

Table 3.5. Peak value from single bit response comparison: Megtron7 (differential).

		Measure	bv-foil	bv-avg	ADS
Peak value (mV)	DM	390.6	420.6	393	370.2
	CM	202.1	221.1	204.8	201.9
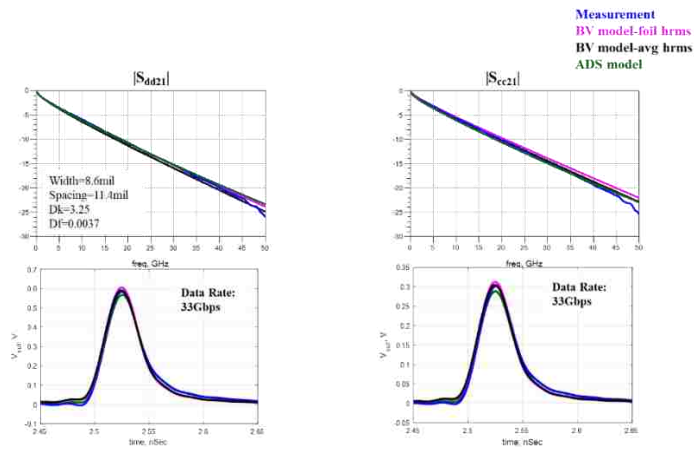
Figure 3.16. Comparison among measurements, behavioral model and ADS model on frequency domain and time domain: DVN material (differential).

Table 3.6. Peak value from single bit response comparison: DVN (differential).

		Measure	bv-foil	bv-avg	ADS
Peak value (mV)	DM	584.3	605.5	590.3	567.7
	CM	302	312.3	304.3	290

A single bit response pick values summary about all validated cases for differential pairs are list in Table 3.7.

Table 3.7. Single bit response peak value comparison between measurements and behavioral model.

Board	Differential mode				Common mode			
	Measure	BV-foil	BV-avg	ADS	Measure	BV-foil	BV-avg	ADS
Panasonic Meg6 HVLP	425	415.8	411.5	423	213	216.9	214.6	217.1
Panasonic Meg6 RTF	390.6	420.6	393	370.2	202.1	221.1	204.8	201.9
Panasonic Meg6 STD	336.3	343.6	338.5	353	175	177.7	175	183
TACHYON -100G VLP2	584.3	605.5	590.3	567.7	302	312.3	304.3	290
TU933	579	582.3	564.9	549	290	301.9	292.8	279

Finally, rms error in percentage is calculated based measurements for behavioral model and ADS model, which is illustrated in Table 3.8. As we can see, behavioral model with average roughness value from foil side and oxide side has error 9.25% when comparing with measurements. However, behavioral model with surface roughness from foil side only have error 17.3% and ADS model has rms error 19.36%. Both of these two model have almost double error than behavioral model with surface roughness considered from both side. Therefore, the conclusion is that the behavioral model can capture material and surface roughness dispersion more accurate, no matter for single-ended transmission line or differential transmission line

Table 3.8. Rms error based on measurement results comparison between behavioral model and ADS model.

Differential mode			Common mode		
BV-foil	BV-avg	ADS	BV-foil	BV-avg	ADS
17.3%	9.25%	19.36%	11.24%	2.41%	8.32%

4. SPHYSIC BASED DIELECTRIC MODEL WITH HURAY MODEL

4.1. MODEL DESCRIPTION

In order to simulate accurately in both frequency domain and time domain, an additional term is added to capture material dispersion behavior. In this proposed method, dielectric model is developed based on Djordjevic model and surface roughness is model by Huray model. The work flow for physic based dielectric model is shown in Figure 4.1.
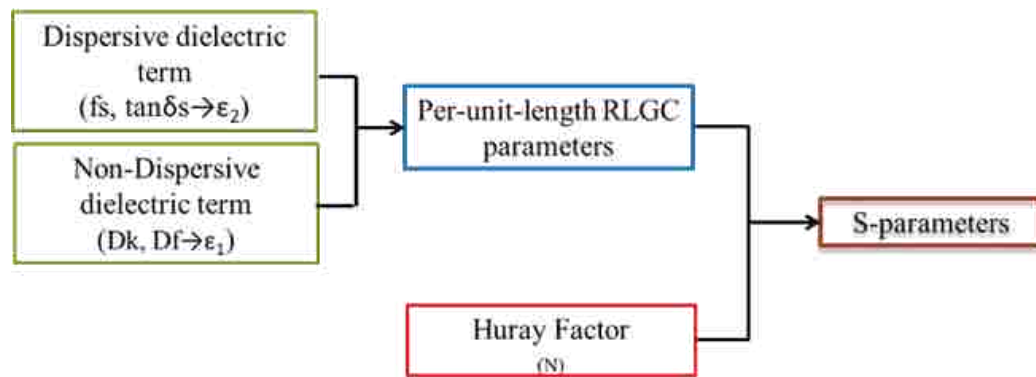
Figure 4.1. Proposed physic based dielectric model with Huray model.

Similar to Behavioral model, we can also calculate bulk dielectric parameter and dispersive term by Djordjevic model. The difference is in behavioral model, the dispersive term already considers surface roughness. The physic based dielectric model only but including surface roughness by using Huray model.

4.2. MODEL PARAMETERS EXTRACTION

According to Equation (26), there are three critical parameters to calculate huray model correction parameter: snowball radius (a), tile dimension (Ahex) and number of snowball (N) [18]. An example of Huray model is shown in Figure 4.2.
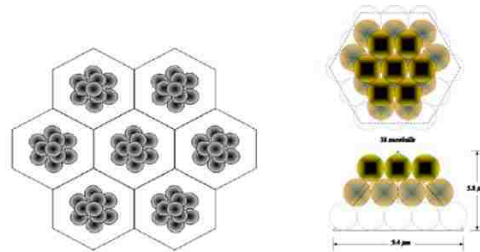
Figure 4.2. Huray model explanation.

$$K_{Huray} = \frac{Prough}{Psmooth} = 1 + \left. \frac{3}{2}\left(\frac{N4\pi a^2}{A_{hex}}\right) \middle/ \left(1 + \frac{\delta}{a} + \frac{\delta^2}{2a^2}\right) \right. \tag{26}$$

Based on Figure 4.3[19], Gould snowball radii distribution of treated drum side from SEM method is:
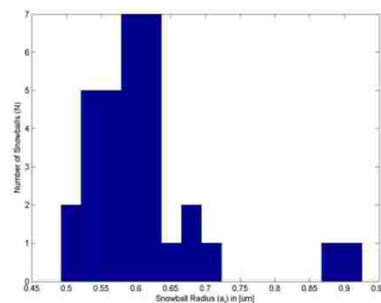
Figure 4.3. Gould snowball radii distribution of threated drum side from SEM method.

Therefore, we can fix snowball radius with a=0.63µm and tile dimension and tile dimension A_{hex}=90µm² to simplify parameter calculation. Till now, Huray model correction factor only depends on snowball number and frequency. Figure 4.4 shows an example that how does Huray correction factors with different snowball number change with frequency:
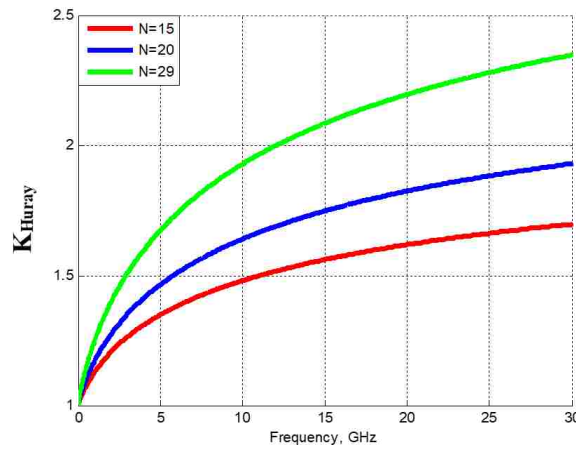
Figure 4.4. Huray correction factor with different number of snowball against frequency.

To use Huray correction factor, we can just simply multiply it with p.u.l resistance based on Equation (27).

$$R_{Huray}(f) = \begin{cases} K_{Huray} R_s \sqrt{f} & \text{when } \delta < t \\ R_{dc} & \text{when } \delta \geq t \end{cases}$$

(27)

In this new dielectric model, the assumption is same material has same dispersion behavior. Therefore, in extraction set, fs and tanδs should be exactly same. Another assumption is same foil type should have same number of snowball. Therefore, twelve

Meg6 boards, which have 3.5mil, 9.5mil, 13mil and 15mil trace width and different foil

type HVLP, VLP/RTF and STD, have same fs and tands and 3 different N numbers. The

correlation between tuned model parameters and measurement is shown in Figure 4.5.

When model other materials, a normalization is needed to do based on bulk Df, which is

also called Df1 in the model.
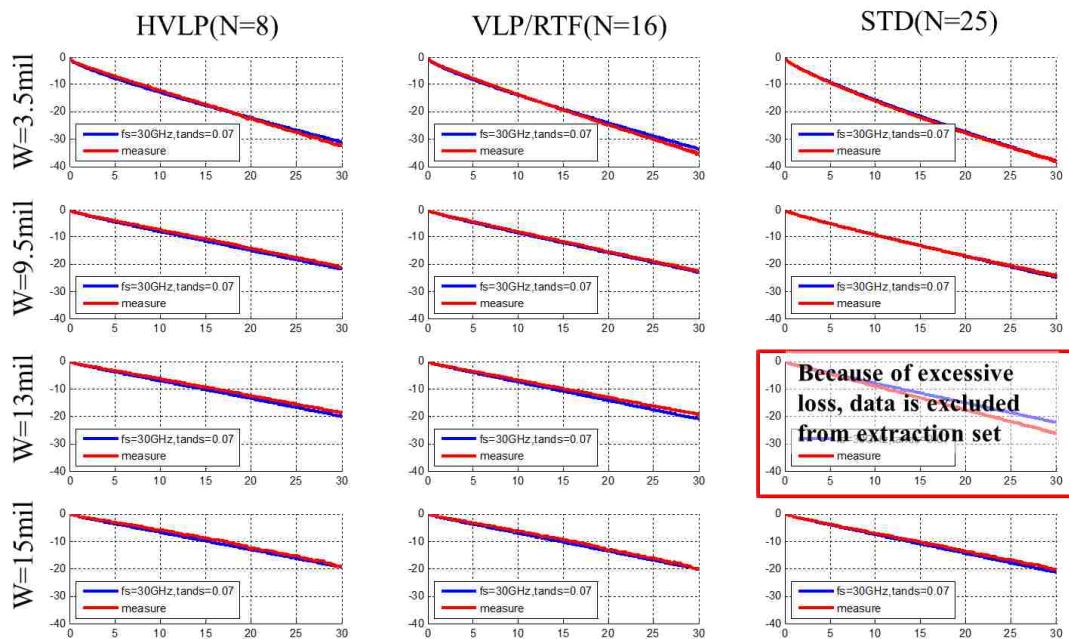
Figure 4.5. Model parameter extraction based on Megtron6 PCBs.

4.3. CURVE FITTING FOR SURFACE ROUGHNESS

As we know, surface roughness can vary from boards to boards due to different

foil type. Even with same foil type, surface roughness can be different due to different

manufactures. Therefore, to solve this issue, curve fitting is done based on extraction set

and equation is: $N=12.95rms^2+13.75rms+3.95$. The curve fitting based on extraction set

is shown in Figure 4.6. The corresponded roughness number and number of snowball are list in Table 4.1.

Table 4.1. Snowball number against surface roughness.

Foil Type	HVLP	VLP/RTF	STD
hrms(um)	0.24	0.57	0.85
N	8	16	25
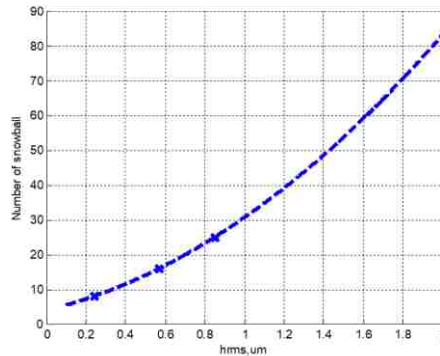
Figure 4.6. Curve fitting for number of snowballs against surface roughness.

Therefore, once surface roughness, which represent by rms value is fixed, is known, number of snowball is known from the fitted curve.

4.4. MODEL VALIDATION AND COMPARISON WITH BEHAVIORAL MODEL (SINGLE-ENDED MODEL)

The comparison among measurements, physic based Huray model and ADS model are done. Two examples are shown based on Megron7 and Doosan-DVN materials in Figure 4.7 and Figure 4.8.
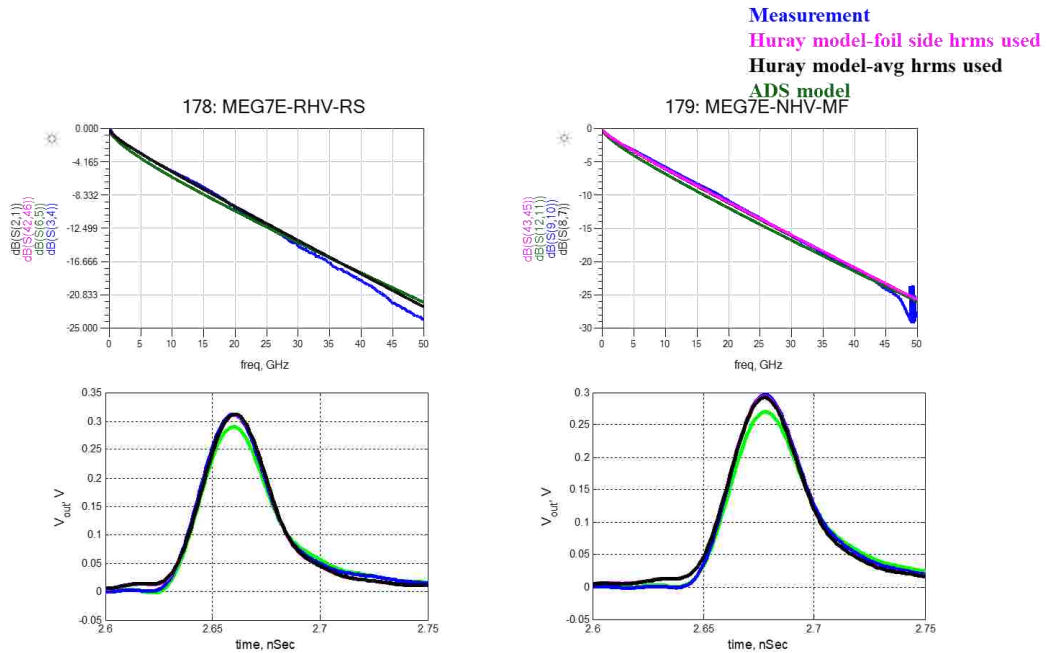
Figure 4.7. Comparison among measurements, behavioral model and ADS model on frequency domain and time domain: Megtron7 material (physic based model).

Table 4.2. Snowball number against surface roughness (Megtron7).

		Measure	Huray-foil	Huray-avg	ADS
Peak value (mV)	178	312	311.3	312.1	290
	179	296	293.5	291.7	270

Table 4.2 and Table 4.3 list peak values of single-bit response form Megtron7 and DVN material. As we can see, Huray model with average roughness value included have better results than other models. Table 4.4 list peak values in millivolt from all validated materials and compared with measurements. Table 4.5 list rms error in percentage. Huray

model with average roughness considered has less error, only 5.98% when comparing

with measurement results.
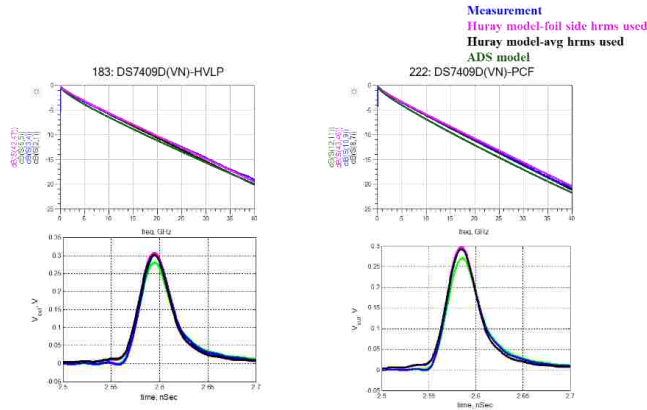
Figure 4.8. Comparison among measurements, behavioral model and ADS model on frequency domain and time domain: DVN material.

Table 4.3. Snowball number against surface roughness (DVN).

		Measure	Huray-foil	Huray-avg	ADS
Peak value (mV)	183	302.2	306.8	300.6	279.7
	222	293.3	298.5	291.9	269.5

Table 4.4. Single bit response peak values comparison among measurement, behavioral model, physical based dielectric model and ADS.

Board	measure	BV-foil	BV-avg	Huray-foil	Huray-avg	ADS
MEG7E-RHV-RS	312	323	320	311.3	312.1	290
MEG7E-NHV-MF	296	302	297	293.5	291.7	270
MEG7NE-RHV-RS	324.7	328.5	325.1	316	317.2	287.5
MEG7NE-NHV-MF	347	363.8	361.1	350	351.2	318.9
DS-7409D (VN)_HVLP	302.2	317	306.3	306.8	300.6	279.7
DS-7409D(V-N)_PCF	293.3	308.5	295.1	298.5	291.9	269.5
DS-7409D(VN)_VO	324.7	327	320.3	315.5	312.9	287.1
DS-7409D(VN)_HO	340.8	350.4	345.8	336.8	335.4	311.6
TACHYON -100G VLP2	301.8	321.1	316.4	313.6	309.7	278.4
TU933	308.3	328.4	321.8	316.8	313.8	294.3

Table 4.5. RMS error comparison among behavioral model, physical based dielectric model and ADS based on measurements.

bv-foil	bv-avg	huray-foil	huray-avg	ADS
13.33	8.51	6.72	5.98	27.23

5. HIGH SPEAD TIGHT COUPLING TEST COUPON WITH NON-FUNCTIONAL DESIGN

According to paper [20], a new method is developed to extract Dk and Df with strong coupling transmission lines. However, most of PCB boards from industries are built with weak coupling traces. Therefore, a test coupon is design with tight coupling traces are designed.

5.1. DESIGN SPACE INVESTIGATION

According to requirements, the test coupon should meet following criteria:

- The differential transmission lines must be strong coupling, which is defined the ration of spacing to dielectric height is less than 1.

- Target impedances are 100ohm, 95ohm or 92ohm.

  - o 100ohm transmission line have trace width around 10mil

  - o 95ohm or 92ohm transmission line have trace width around 4mil

- Board thickness should be around 93mil

  Base on the criteria above, by sweeping trace width and spacing with:

- Core thickness: 4mil

- Prepreg thickness: 4.32mil

- Trace thickness: 0.6mil

- Glasstype: 1035 with 2ply

- Resin content: 72%

- Dk: 3.15 @1GHz

- Df: 0.003 @1GHz

The design space is developed as shown in Figure 5.1.
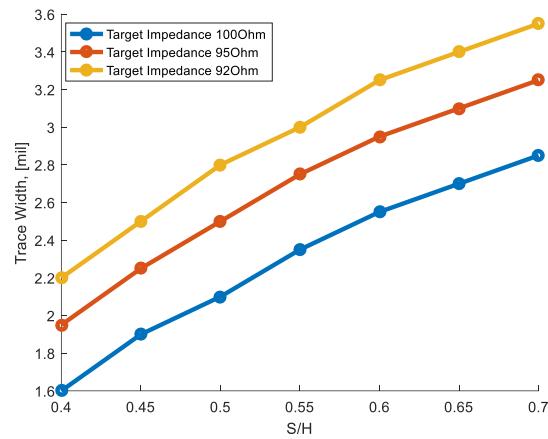
Figure 5.1. Design space for strong coupling test coupon.

Table 5.1. Calculated trace width and spacing against target impedance.

S/H	Spacing [mil]	LW [mil], 100Ohm	LW [mil], 95Ohm	LW [mil], 92Ohm
0.4	1.73	1.6	1.95	2.2
0.45	1.94	1.9	2.25	2.5
0.5	2.16	2.1	2.5	2.8
0.55	2.38	2.35	2.75	3
0.6	2.59	2.55	2.95	3.25
0.65	2.81	2.7	3.1	3.4
0.7	3.02	2.85	3.25	3.55

However, based on manufacturing limitations, the most narrow trace width can be done is 3mil. Therefore, only combinations in Table 5.1 with green can be considered.

Before doing next step, it is better to check whether the geometries selected are good to do Dk and Df extraction with new method.
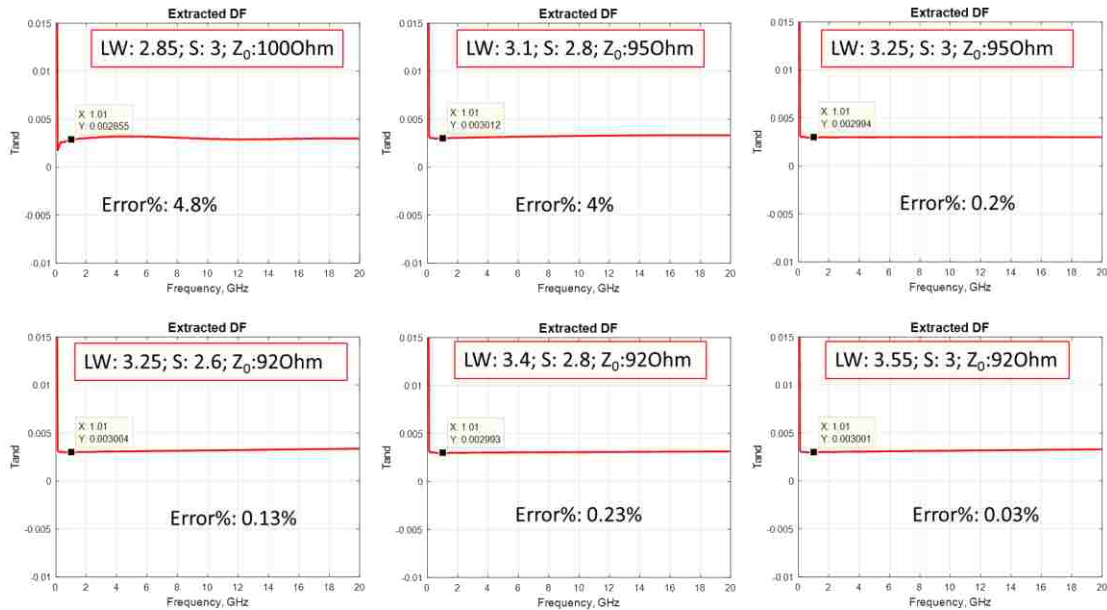
Figure 5.2. Error percentage for different trace width and spacing.

By using simulated S-parameters to do extraction, all extracted Df has error percentage within 5%, as shown in Figure 5.2. Therefore, any geometries list above are good to go next step.

5.2. PROPOSED STACKUP

According to requirement, the stackup should have at least 10 layers as shown in Figure 5.3.

In addition, surface roughness on traces and ground should be comparable. Otherwise, higher surface roughness on ground will generate additional loss. Therefore,

this situation should be avoid. The make sure PCB builder will not mess up it, another

two layers are added to most top and bottom. Therefore, there are totally 12 layers.

1	————————————	GND
2	———	100Ohm Signal Layer
3	————————————	GND
4	———	95Ohm Signal Layer
5	————————————	GND
6	————————————	GND
7	———	95Ohm Signal Layer
8	————————————	GND
9	———	100Ohm Signal Layer
10	————————————	GND

Figure 5.3. Proposed stackup.

After discussing with PCB vendors, the finished trace width are shown in Table

5.2.

Table 5.2. Calculated trace width and spacing against target impedance from vendor.

Target Impedance Trace width	Single ended	Differential(Trace width/Spacing)
95Ohm	4.5mil	3.5mil/2.75mil
100Ohm	12.75mil	9.25mil/8.55mil

Then, the finalized stackup is shown in Figure 5.4. For signal layer 5 and layer 8, stackup is symmetric with 4mil dielectric height and for signal layer 3 and layer 10, dielectric height for core prepreg are 10mil and 12mil, separately.

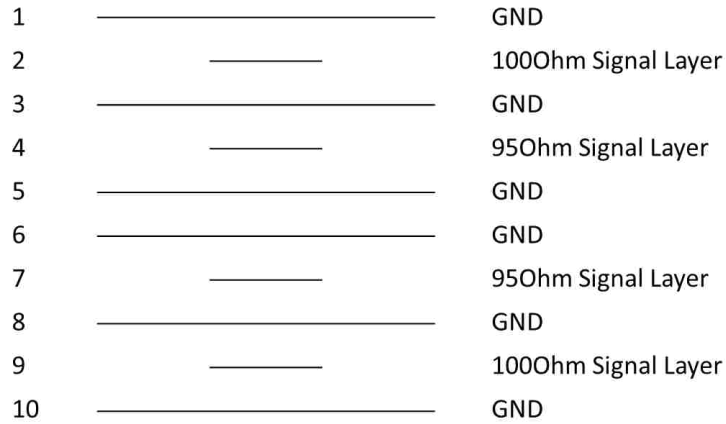| Lyr	Lyr Type	Image	Foil Wt	Cu Type	Thk (mil)	Cu Thk	Er	Generic Name	Construction	RC%	Material Family
L1sm					1.20		3.5				
L1	Sig		1/2oz			1.8	3.2	0.50 oz - Foil			Foil MEG7N
					3.90		3.2	3313 HF (59%)		59	
L2	Pln		1oz	HVLP2	10.00	1.2	3.2	0.01 HHxH1	2x2116	55	MEG7N
L3	Sig		1/2oz	HVLP2		0.6	3.2	3313 HF (59%)		59	MEG7N
					12.00		3.2	3313 HF (59%)		59	MEG7N
							3.2	3313 HF (59%)		59	MEG7N
L4	Pln		1/2oz	HVLP2	4.00	0.6	3.1	0.004 HHxHH	2x1035	67	MEG7N
L5	Sig		1/2oz	HVLP2		0.6	3	1035 HF (72%)		72	MEG7N
					4.00		3	1035 HF (72%)		72	MEG7N
L6	Pln		1/2oz	HVLP2	10.00	0.6	3.2	0.01 HHxHH	2x2116	55	MEG7N
L7	Pln		1/2oz	HVLP2		0.6	3	1035 HF (72%)		72	MEG7N
					4.00		3	1035 HF (72%)		72	MEG7N
L8	Sig		1/2oz	HVLP2	4.00	0.6	3.1	0.004 HHxHH	2x1035	67	MEG7N
L9	Pln		1/2oz	HVLP2		0.6	3.2	3313 HF (59%)		59	MEG7N
					12.00		3.2	3313 HF (59%)		59	MEG7N
							3.2	3313 HF (59%)		59	MEG7N
L10	Sig		1/2oz	HVLP2	10.00	0.6	3.2	0.01 HHxH1	2x2116	55	MEG7N
L11	Pln		1oz	HVLP2		1.2	3.2	3313 HF (59%)		59	MEG7N
					3.90		3.2	3313 HF (59%)		59	MEG7N
L12	Sig		1/2oz			1.8	3.2	0.50 oz - Foil			Foil
L12sm					1.20		3.5				

Figure 5.4. Finalized stackup by vendor.

5.3. VIA OPTIMIZATION

In order to make sure return loss is less than -20dB at Nyquist frequency, via optimizations are done in HFSS separately for 95ohm via and 100ohm via, which are for layer5 and layer8, layer3 and layer10, separately.

5.3.1. 95ohm Via Optimization. To get less discontinuities, via optimization is pretty important. To simulate real cases, two 2.4mm SMA connector models from SMA

connector vendor are included in optimization. The HFSS simulation model shows in
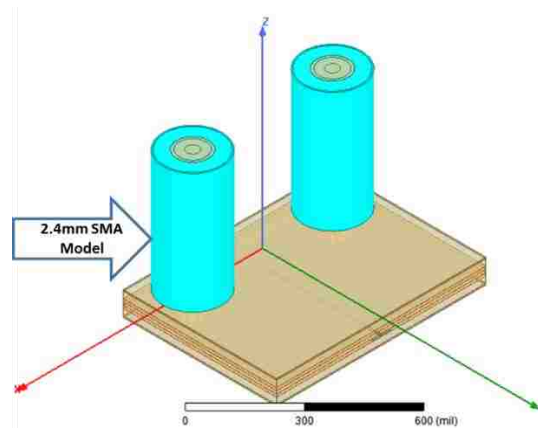
Figure 5.5 and Figure 5.6.

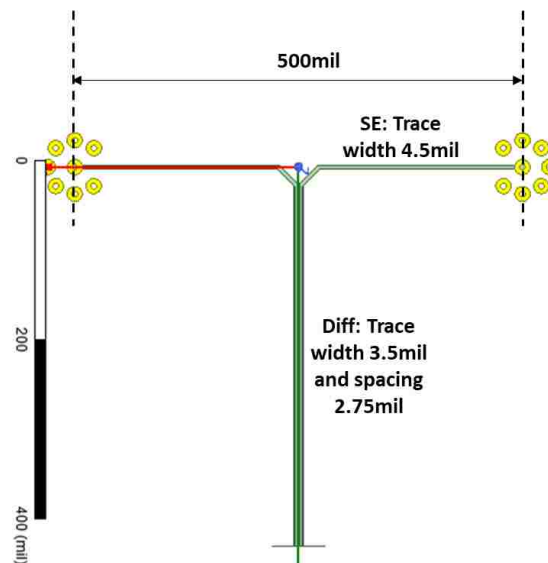Figure 5.5. HFSS model with 2.4mm SMA connectors included.

Figure 5.6. 500mil space between connectors.

Each signal via has 7 ground vias around. The distance between signal via and each related ground via is 30mil to minimize inductance caused by loop from signal via to ground vias. Both signal vias and ground vias have drill hold size 7.9mil and pad size (inner and outer) 17mil. Dielectric constant and dissipation factor are 3.1 and 0.0025, separately. When doing simulation, Djordjevic-Sarkar model also applied to make sure simulation results are closed to real measurement. First, port impedance is checked before full-wave simulation is run, which is shown in Figure 5.7.

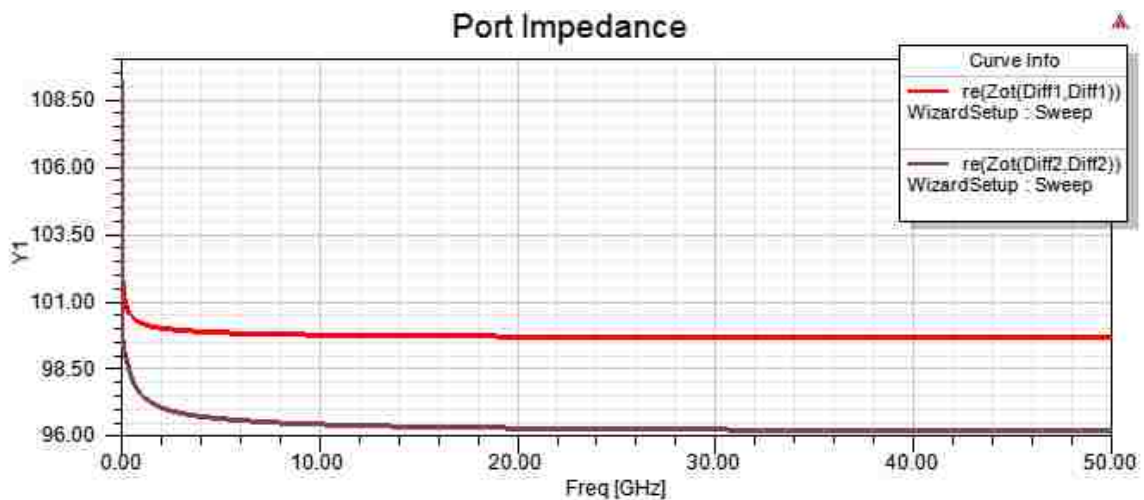Figure 5.7. Port impedance are 100ohm for 2.4mm connector side and 96ohm for trace side.

Diff1 is assigned to 2.4mm SMA connectors side and Diff2 is assigned to trace side. Diff1 has port impedance 100ohm and diff2 has port impedance 96ohm. Both port impedance are closed to target impedance and error is within tolerance percentage. Therefore, full-wave simulations and optimization will be done next.

With regular optimization, via impedance cannot be reduced anymore. This phenomenon is more server for traces located at layer 10 (This part will be introduced in next session). Figure 5.8 shows return loss and TDR with antipad 26mil above signal layer and antipads size sweeping from 32mil to 36mil:
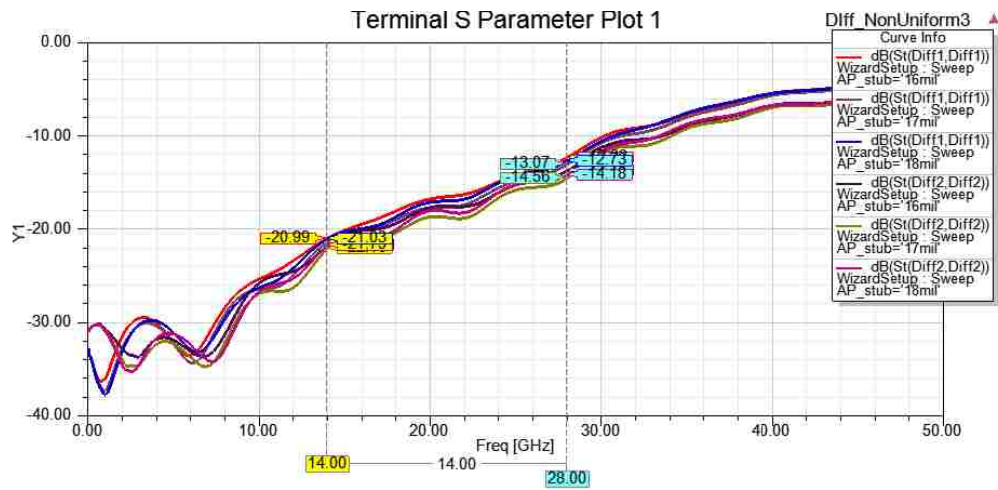
a
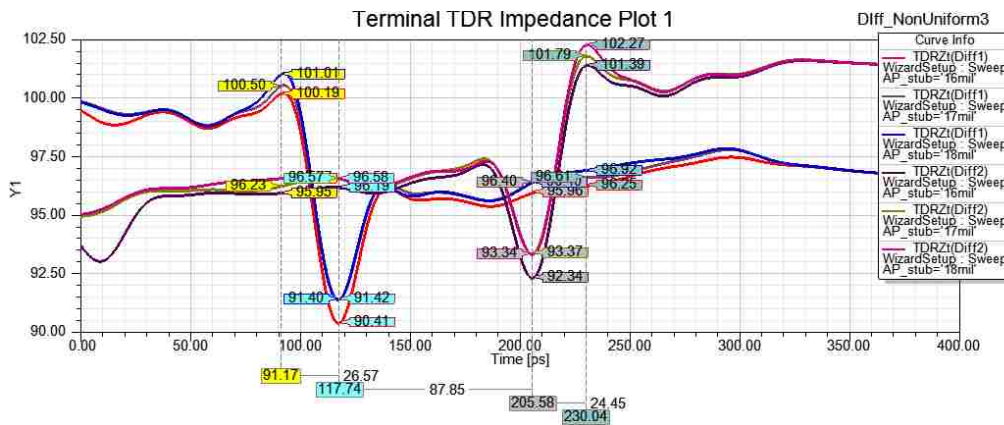
b

Figure 5.8. Simulated S-parameters. a) Return loss. b) TDR.

Because the material, Metron7N, is design for data rate 56Gbps PAM4 data, Nyquist and second harmonic frequency 14GHz and 28GHz are marked in return loss. As we can see, return loss at 14GHz are roughly -21dB and -14dB at 28GHz. To run the test coupon with high data rate, we hope to optimize high frequency more. From TDR results, the dip caused by inner pad at signal layer and antipad an adjacent layer, which is within 5ohm with target impedance. However, a high impedance impact return loss at high frequency. Because the antipad above signal layer is already shrinked to manufacturing limitation, non-functional pads are considered at above layers to help reduce this high impedance.
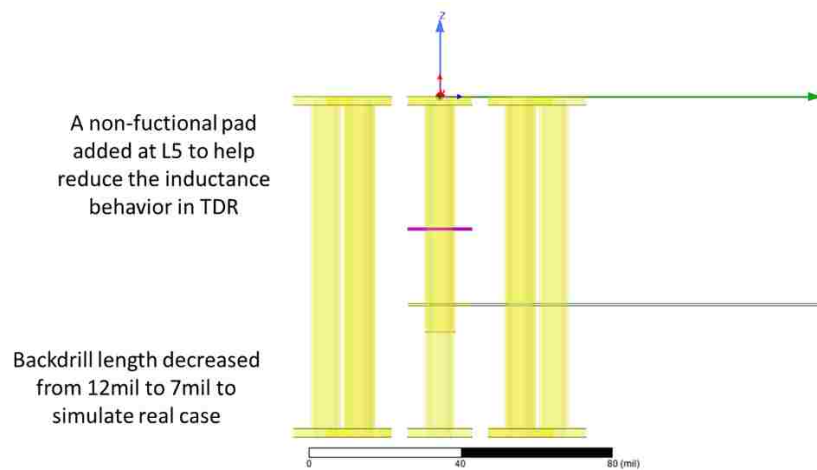
Figure 5.9. An additional non-functional pad is added at layer5.

After add a non-functional pad at layer 5, as Figure 5.9 shown, continue to sweep antipad at adjacent layers from 38mil to 44mil is done. Then, best setting for 95ohm via are:

- Drill hole size: 7.9mil

- Pad size (inner and outer): 17mil

- Signal to ground via distance: 30mil

- Antipad size L1-L7: 26mil

- Antipad size L7-L12: 44mil

Optimized S-parameters and TDR results are shown in Figure 5.10. As we can see, return loss in much belown -20dB and impedance is within 10% tolerance.
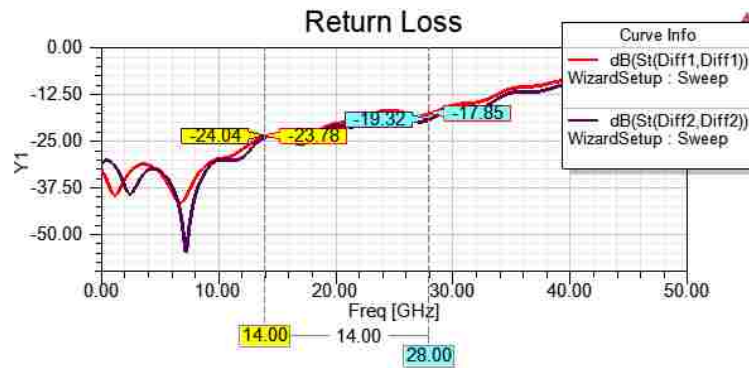
a

b

Figure 5.10. Simulated S-parameters with non-functional pad. a) Return loss. b) Insertion loss. c) TDR.
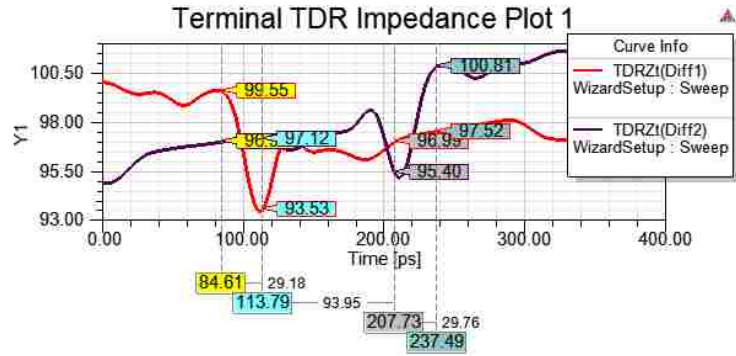
c

Figure 5.10. Simulated S-parameters with non-functional pad. a) Return loss. b) Insertion loss. c) TDR. (Cont.)

After adding non-function pads, return loss at 14GHz decreases from -21dB to -24dB and -13dB to -19dB at 28GHz.

5.3.2. 100ohm Via Optimization. Similar to 95ohm via optimization at layer 8, another optimization is done with 100ohm via at layer 10. HFSS model for 100ohm via is shown in Figure 5.11.
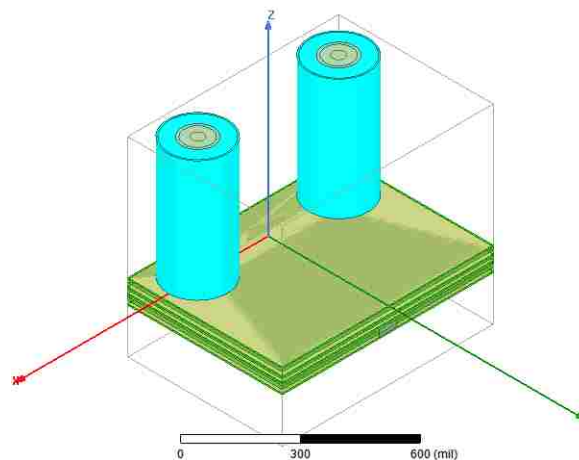
Figure 5.11. HFSS model for 100ohm via optimization, 2.4mm SMA connectors model are included.

Figure 5.12 shows the geometries for 100ohm vias. Those geometries are consistent with 95ohm vias. Trace width is 12.75mil at signal-ended area and 9.25mil at differential area. The distance between two SMA connector (center to center) for one differential pair is 500mil. Based on the new Dk/Df extraction methodology [20], the distance for single-ended area should be as short as possible. Therefore, considering cables diameter, 500mil is the closest distance can be used. There are seven ground vias around one signal via. The distance between ground via and signal via is 30mil. A non-functional pad also added at layer 3 to help reduce high impedance, which is shown in Figure 5.13.

a   b
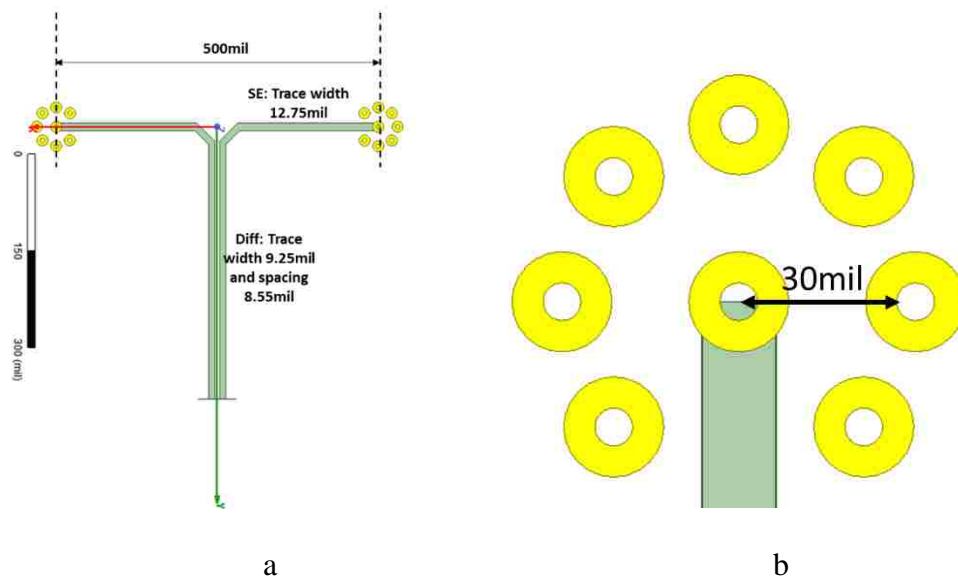
Figure 5.12. HFSS model geometries. a) 500mil spacing between two connectors. b) Distance between signal via to ground via is 30mil.
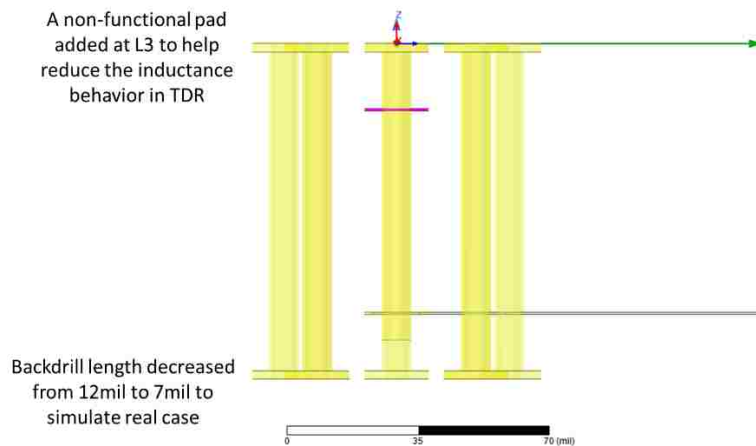
Figure 5.13. An additional non-functional pad is added at layer3.

To make sure discontinuities not coming from traces mismatch, port impedance is

checked before 3D full wave simulation, which is shown in Figure 5.14.
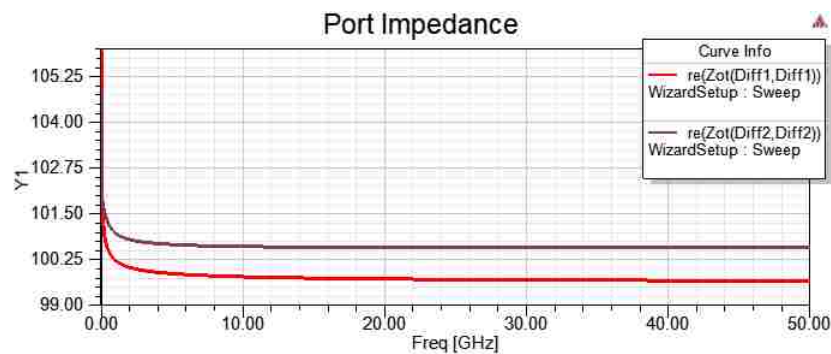
Figure 5.14. Port impedance check: 100ohm for both connector side and trace side.

Diff 1 is assigned to 2.4mm SMA connectors side and Diff 2 is assigned to traces

side. For both side impedance are closed to 100ohm. Therefore, we can do optimization

based on current geometries.

After sweeping antipad size at adjacent layers, the best results are shown in Figure 5.15.
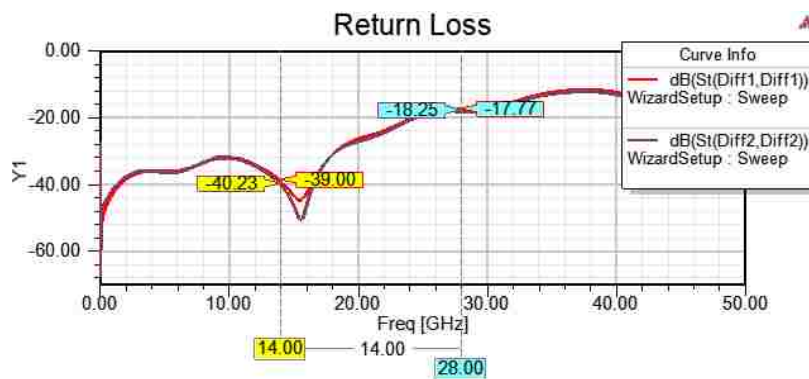
a
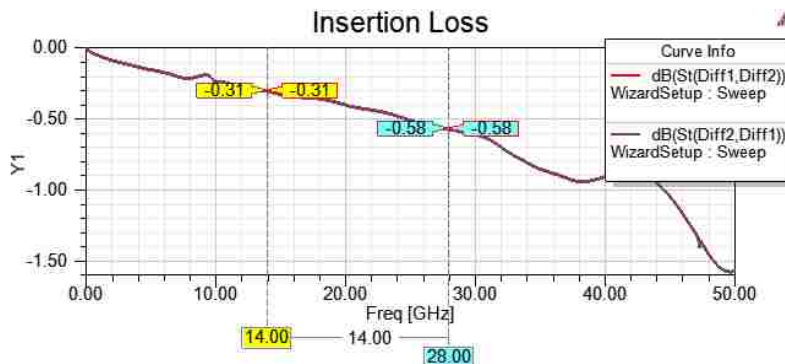
b
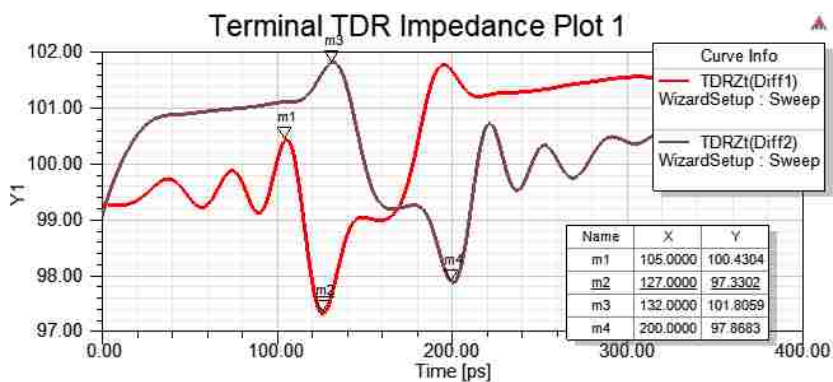
c

Figure 5.15. Simulated results from HFSS. (a) Return loss. b) Insertion loss. c) TDR.

Return loss at 14GHz is -40dB and even at 28GHz is -18dB. TDR also shows that impedance is controlled within ±3Ohm comparing with target impedance. Therefore, summarize geometries are:

- Drill hole size: 7.9mil

- Pad size (inner and outer): 17mil

- Signal to ground via distance: 30mil

- Antipad size L1-L8: 26mil

- Antipad size L9-L12: 34mil

5.4. PCB LAYOUT

After figuring out single-ended and differential traces needed on PCB boards, all traces are routed via Cadence Allegro, which is shown in Figure 5.16.
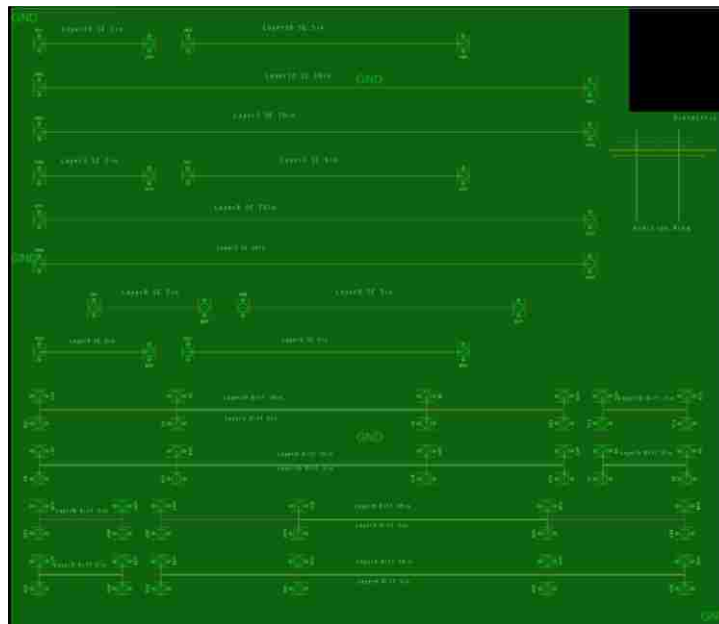
Figure 5.16. PCB layout.

A 13in $\times$ 11.25in PCB is designed. In this PCB board, both single-ended and differential pairs at layer3, layer5, layer8 and layer11 are included. Besides all testing traces, there are another two areas are included:

On the top right corner, an 1800mil $\times$ 1900mil dielectric area is designed for doing SPDR measurements. In this area, all copper layers are removed. By comparing the Df value measured by SPDR measurements and extracted from S-parameters, the difference will clearly show how does surface roughness impact transmission line loss. Below the dielectric area, a cross-section area is also designed. Both single-ended and differential traces at layer8 and layer10 are included this area. Therefore, there is no need to damage any traces used for testing but just cut the artificial ones.

BIBLIOGRAPHY

[1] Stephen H. Hall, Howard L. Heck. "Advanced Signal Integrity for High – Speed Digital Design" [Online] Available: http://onlinelibrary.wiley.com/book/10.1002/9780470423899

[2] John David Jackson. Classical Electrodynamics. John Wiley & Sons Ltd. 1962.

[3] Lee, B. "The Impact of Innerlayer Copper Foil Roughness on Signal Integrity", Printed Circuit Design and Fab, April 200.

[4] Xinyao Guo, Han Gao, Guangyao Shen, Qian Liu, Victor Khilkevich, James Drewniak, Soumya De, Scott Hinaga, Douglas Yanagawa, "Design methodology for behavioral surface roughness model", Electromagnetic Compatibility (EMC) 2016 IEEE International Symposium on, pp. 927-931, 2016.

[5] Djordjevic A.R.; Biljie, R.M.; Likar-Smiljanic, V.D.; Sarkar, T.K., "Wideband frequency-domain characterization of FR-4 and time-domain causality," in Electromagnetic Compatibility, IEEE Transactions on , vol.43, no.4, pp.662-667, Nov. 2001 doi: 10.1109/15.97464.

[6] A.V. Rakov, S. De, M. Y. Koledintseva, S. Hinaga, J. L. Drewniak and R. J. Stanley, "Quantification of Conductor Surface Roughness Profiles in Printed Circuit Boards," in IEEE Transactions on Electromagnetic Compatibility, vol.57, no. 2, pp. 264-273, April 2015.

[7] Ippich, "A Designs Experiment for the Influence of Copper Foils on Impedance, DC Line Resistance and Insertion Loss," IPC APEX Expo 2012.

[8] Y. Shlepnev, "Dielectric and Conductor Roughness Models Identification for Successful PCB and Packaging Interconnect Design up to 50 GHz," The PCB Design Magazine 02/2014; 2014(2):12-28.

[9] Koledintseva, M.Y.; Razmadze, A.G.; Gafarov, A.Y.; Soumya De; Drewniak,J.L.; Hinaga, S., "PCB conductor surface roughness as a layer with effective material parameters," in Electromagnetic Compatibility (EMC), 2012 IEEE International Symposium on , vol., no., pp.138-143, 6-10 Aug. 2012.

[10] https://en.wikipedia.org/wiki/Effective_medium_approximations

[11] http:/ningpan.net/publications/151-200/156.pdf

[12] S. G. Pytel, G. Barnes, D. Hua, A. Moonshiram, G. Brist, R. Mellitz, S. Hall, and P. G. Huray, "Dielectric modeling, characterization, and validation up to 40GHz," presented at the 11th Signal Propag. on Interconnects Workshop, Genoa, Italy, May 13–16, 2007.

[13] Deutsch, e.t. "Extraction of ε_r(f) and tanδ(f) for Printed Circuit Board Insulators Up to 30 GHz Using the Short-Pulse Propagation Technique," IEEE Transactions on Advanced Packaging, vol.28, no.1, Feb. 2005.

[14] Lei Hua, Bichen Chen, Shuai Jin, Marina Koledintseva, Jane Lim, Kelvin Qiu, Rick Brooks, Ji Zhang, Ketan Shringarpure, Jun Fan, "Characterization of PCB dielectric properties using two striplines on the same board," in Electromagnetic Proc. IEEE Int. Symp. EMC Raleigh, pp. 809-814, Aug. 4–8, 2014.

[15] S.B. Cohn. "Shielded Coupled-Strip Transmission Line". IRE Transactions on Microwave Theory and Techniques. October, 1955.

[16] Harold A. Wheeler, 'Formulas for Skin Effect', Proceeding of the I.R.E, Sep 1942.

[17] Jeonghyeon Cho. "Mixed-Mode ABCD Parameters: Theory and Application to Signal Integrity Analysis of PCB-Level Differential Interconnects". IEEE Transactions on Electromagnetic Compatibility. Vol 53 August, 2011.

[18] Paul G. Huray. "Impact of Copper Surface Texture on Loss: A model that Works". DesignCon. 2010.

[19] Michael Griesi. "Eletrodeposited Copper Foil Surface Characterization for Accurate Conductor Loss Modeling". DesignCon. 2015.

[20] Shaohui Yong, Yuanzhuo Liu, Han Gao, Bichen Chan, Soumya De, Scott Hinaga, Douglas Yanagawa, James Drewniak, Victor Khikcvich, "Dielectric Dissipation Factor (DF) Extraction Based on Differential Measurements and 2-D Cross-sectional Analysis," in Electromagnetic Compatibility (EMC) 2018 IEEE International Symposium.

[21] X. Sun, T. Huang, L. Ye, Y. Sun, S. Jin, and J. Fan, "Analyzing Multiple Vias in a Parallel-Plate Pair Based on a Nonorthogonal PEEC Method" IEEE Transactions on Electromagnetic Compatibility, 2018.

[22] B. Chen, J. He, X. Sun, Y. Guo, S. Jin, and J. Fan, "Differential S-Parameter De-embedding for 8-Port Network", 2018 IEEE Symposium on Electromagnetic Compatibility, Signal Integrity and Power Integrity (EMC, SI & PI), Long Beach, CA, USA.

[23] X. Sun, L. Ye, K. Song, Y. Sun, S. Jin, B. Chen, M. Tsiklauri, X. Ye, and J. Fan "An Efficient Approach to Find the Truncation Frequency for Transmission Line-Based Dielectric Material Property Extraction" 2018 IEEE Symposium on Electromagnetic Compatibility, Signal Integrity and Power Integrity (EMC, SI&PI), Long Beach, CA, USA.

[24] S. Jin, D. Liu, B. Chen, R. Brooks, K. Qiu, J. Lim, and J. Fan, "Analytical Equivalent Circuit Modeling for BGA in High-Speed Package" IEEE Transactions on Electromagnetic Compatibility. Vol. 60, pp 68-76, Feb 2018.

[25] S. Jin, D. Liu, Y. Wang, B. Chen and J. Fan "Parallel Plate Impedance and Equivalent Inductance Extraction Considering Proximity Effect by a Modal Approach", IEEE Transactions on Electromagnetic Compatibility. Vol. 60, pp 1481-1490, Oct 2018.

[26] S. Jin, B. Chen, X. Fang, H. Gao and J. Fan, "Improved "Root-Omega" method for transmission-line based material property extraction for multilayer PCBs", IEEE Trans. On Electromagnetic Compatibility. Vol. 59, pp 1356-1367, Aug 2017.

[27] L. Ye, C. Li, X. Sun, Shuai Jin, B. Chen, X. Ye, and J. Fan, "Thru-Reflect-Line Calibration technique: error analysis for characteristic impedance variations in the line standards," IEEE Trans. On Electromagnetic Compatibility. Dec. 2017.

[28] S. Jin, "Modal based BGA modeling in high-speed package", dissertation in Thesis in Missouri University of Science and Technology, 2017.

[29] S. Jin, J. Zhang, J. Lim, K. Qiu, R. Brooks, and J. Fan, "Analytical Equivalent Circuit Modeling for Multiple Core Vias in a High-Speed Package," in Proc. IEEE Int. Symp. EMC, Ottawa, CN, July. 25-29, 2016

[30] B. Chen, M. Tsiklauri, C. Wu, Shuai Jin, J. Fan, X. Ye and B. Samaras, "Analytical and numerical sensitivity analyses of fixtures de-embedding," in Proc. IEEE Int. Symp. EMC, Ottawa, CN, July. 25-29, 2016

[31] S. Jin, X. Fang, B. Chen, H. Gao, X. Ye and J. Fan, "Validating the transmission-line based material property extraction procedure including surface roughness for multilayer PCBs using simulations," in Proc. IEEE Int. Symp. EMC, Ottawa, CN, July. 25-29, 2016.

[32] S. Jin, J. Zhang and J. Fan, "Optimization of the transition from connector to PCB board," in Proc. IEEE Int. Symp. EMC, Aug. 5-9, 2013.

VITA

Han Gao received her M.S. degree of Statistics in May 2013 from Rutgers University, New Brunswick. She joined the EMC Lab for her second M.S degree. She received her M.S. degree of Electrical Engineering in May 2019 from Missouri University of Science and Technology. She had a co-op in Cisco Enterprise Switching Access team from January to December 2017.

Her research interests included signal integrity in high-speed digital system, surface roughness and dielectric model investigation, lossy material properties, SerDes characterizations.